THESIS

THE ROLE OF FLNC IN THE CONTRACTILITY OF THE HEART AND VALVE DEVELOPMENT IN ZEBRAFISH

Submitted by

Areej Ali Alshahrani

Department Of Biology

In partial fulfillment of the requirements

For the Degree of Master of Science

Colorado State University

Fort Collins, Colorado

Spring 2020

Master's Committee:

Advisor: Deborah Garrity
Rachel Mueller
David Bark

ABSTRACT

THE ROLE OF FLNC IN THE CONTRACTILITY OF THE HEART AND VALVE DEVELOPMENT IN ZEBRAFISH

Dilated Cardiomyopathy (DCM) is the most common type of cardiomyopathy disease that causes heart muscle defects. DCM is characterized by a dilated left ventricular chamber and systolic dysfunction that results in congestive heart failure. Although the cause of DCM is not fully understood, evidence supports the hypothesis that costameric proteins contribute to muscle dysfunction linked to cardiomyopathy. In fact, the mutation of *FLNC* has been linked to many muscle disease including myofibrila myopathies (MFM) and different types of cardiomyopathy. However, the mechanisms underlying the variability between MFM and cardiac disease is a filed of interest. Patients with DCM showen to carry truncating variants whereas patients with hypwetrophic cardiomyopathy (HCM) carried missense variants. Additionaly, patiants with other types of cardiomyopathy carried missense or in-frame indel variants(Ader, Groote et al.). This seems to suggest that different mechanisms may be at play regarding the role of FLNC in cardiac developmens and they remain unclear. It would be interesting to examine if a similar correlation holds in animal model like zebrafish. Therefore, our group has developed the zebrafish model for study of the *FLNC* contribution to cardiac phenotypes. Here, we used several *FLNC* mutant lines to investigate how FLNC directly or indirectly affects development of the atrioventricular (AV) valve. To date, little data indicate whether or not increased RFF is pathologic. This project will test the overarching hypothesis that *flnc* depletion causes changes in RFF, which lead to aberrant valve development, which in turn affects overall heart function. We find that the cardiac

morphological phenotype of most single *FLNC* alleles showed normal heart pharameters such as heart rate, stroke valume, cardiac output and reverse flow fraction. However, *flcnb* $^{exon\ 14-/-}$ allele exhibited a decreased in stroke volum and cardiac output whereas RFF is intact. Furturemore, using a immunocytochemistry to examine a correlation that may exist between the strength of the cardiac phenotype and the presence of valve defects indicate that valve defects presented in *flncb* truncation mutants, and suggest that defects in *flncb*$^{exon35-/-}$ embryos are more severe. In support of this finding, our qPCR study displayed that expression levels of *klf2a* and *klf2b* in *flnca*$^{exon1-/-}$ *; flncb*$^{exon14-/-}$ double mutant hearts were significantly decreased. In addition, Prior studies have proposed that massive formation of intracellular protein aggregates imposes toxic impacts that contribute to the skeletal muscle degeneration observed in myofibrillar myopathy (Fichna, Maruszak et al. 2018). We demonstrated that the truncated protein either exerts a direct toxic effect, and/or sequesters wildtype FLNC leading to insufficiency phenotypes.

ACKNOWLEDGMENTS

I would like to thank God for assisting me along in my journey. My completion of this project could not have been accomplished without the support of my family in my education and prepartion for my future with all love, prayers, caring and sacrifices.

I would like to pay my special regards to my adviser Dr. Deborah Garrity for giving me the opportunity to do research and providing invaluable guidance that helped me throughout the time of research and writing of this thesis. It was an awesome privilege and honor to work and study under her guidance. Besides my adviser, I would like to give thanks to my committee members for their encouragement and insightful comments.

I am extending my thanks to Alex Gendernalik for his help in using the high speed camera and Matlab. I would like also to say thanks to my friends and research colleagues in Garrity lab (graduate and undergraduate students) for their constant encouragement.

Lastly, I thank the Saudi Arabian Cultural Mission to the U.S for providing me with a full scholarship to support me financially and spiritually.

TABLE OF CONTENTS

CHAPTER 1: LITERATURE REVIEW

Zebrafish as a model organism:

The zebrafish *Danio rerio* is a small-bodied tropical freshwater fish originally from South Asia which has developed as a prominent vertebrate model organism for the study of genetics, developmental biology and human disease in the last 30 years (Figure 1.1) (Poon and Brand 2013, Meyers 2018). Several attributes have led to its widespread use in research fields and make it particularly powerful for experimental manipulation and developmental studies.

Advantages of the zebrafish system for studies of early development:

The feasibility of genetic screens in zebrafish is enhanced by the small size of adults (approximately 3–5 cm), and the relatively short (3-4 months) time to reproductive maturity. Offspring may be raised easily and bred in captivity. Efficient mutagenesis, transgenesis and genome editing techniques are in place that provide a versatile range of possible genetic manipulations. Forward genetic screens using radiation or chemical treatment to induce mutagenesis represent an unbiased approach to identify genes with fundamental functions, characterized based on their specific mutant phenotypes (Yalcin, Amindari et al. 2017). Reverse genetic approaches including morpholino oligonucleotide injection into the fertilized egg have successfully identified the functions of many known genes (Carpio and Estrada 2006, Asnani and Peterson 2014), although the significant potential for off-target phenotypes represents a limitation to this technique. Increasingly, RNA-guided CRISPR/Cas9- mediated targeted mutagenesis techniques are being used to create both knockout and knock-in alleles. CRISPR/Cas9 provides an increasingly sophisticated way to manipulate the genome in order to develop new models for understanding the pathophysiology of human diseases (Liu, Petree et al. 2019). A variety of tissue-specific transgenic lines are available for studies of early

developmental differentiation. Examples relevant to the cardiac research performed in this study include the *Tg*(*cmlc2-GFP)* (*cmlc2, cardiac myosin light chain 2*, also known as *myl7* – Zebrafish Information Network), which expresses the green fluorescent protein (GFP) specifically in myocardial cardiomyocytes (Huang, Tu et al. 2003, Nguyen, Lu et al. 2008). The transgenic lines used to study the endocardium include *Tg(fli□GFP)* which expresses GFP in all vascular endothelial cells as well as endocardium (Poon, Liebling et al. 2010). A third transgenic line that labels the striated Z discs with EGFP is *Tg*(*cmlc2:Cypher-EGFP*)(Yang and Xu 2012). The number of offspring produced by zebrafish mated pairs is large compared to other vertebrate model organisms; a single mating can fertilize several hundred eggs under ideal conditions. The abundance of offspring allows larger numbers of replicates to be performed simultaneously (Lin, Zhao et al. 2013). The high fecundity of zebrafish is an additional advantage for large-scale genetic approaches (Carpio and Estrada 2006). Large-scale mutagenesis screens performed in laboratories in Tübingen and Boston in the 1990's generated over 4,000 mutations that later resulted in the determination of over 400 genes with defined roles in various aspects of early development (Spence, Gerlach et al. 2008). Once characterized, the zebrafish mutant phenotypes frequently resembled the morphologies and symptoms of human genetic disorders. As one example, the zebrafish *heartstrings* (*hst*), a *tbx5* mutant, is a good disease model for understanding Holt-Oram syndrome, an autosomal, dominant disorder in humans that exhibits a combination of cardiac dysfunction and upper limb malformation (Garrity, Childs et al. 2002). Zebrafish mutant phenotypes in *hst* embryos recapitulate several aspects of Holt-Oram syndrome, including cardiac defects and the lack of upper limbs (pectoral fins). The phenotypes of both zebrafish *hst* embryos and humans with Holt-Oram syndrome are caused by mutation in the T-box transcription factor Tbx5 (Dooley and Zon 2000). Collectively, these advantages

make zebrafish a major platform for conducting genetic screens to identify and characterize genes required for heart development and other embryonic processes(Lin, Zhao et al. 2013).

Characteristic of zebrafish useful for studying developmental biology:

Zebrafish offers certain advantages for the study of early developmental stages in comparison with the mouse. First, fertilization is external in zebrafish whereas in mouse it occurs in utero; thus, zebrafish provides easier experimental access for the study of organ development in live embryos (Dooley and Zon 2000). In addition, the chorionic membrane surrounding the embryo is optically transparent. The chorion is a thick acellular membrane that surrounds the mature eggs and functions as an efficient molecular barrier that protects and isolates the developing embryos from external environmental conditions. For vertebrate models, embryo transparency in the early larval stages of zebrafish is a unique characteristic that allows visualization of the formation and function of internal organs such as heart and neural circuits (Cotelli, Andronico et al. 1988, Ackermann and Paw 2003, Carpio and Estrada 2006).

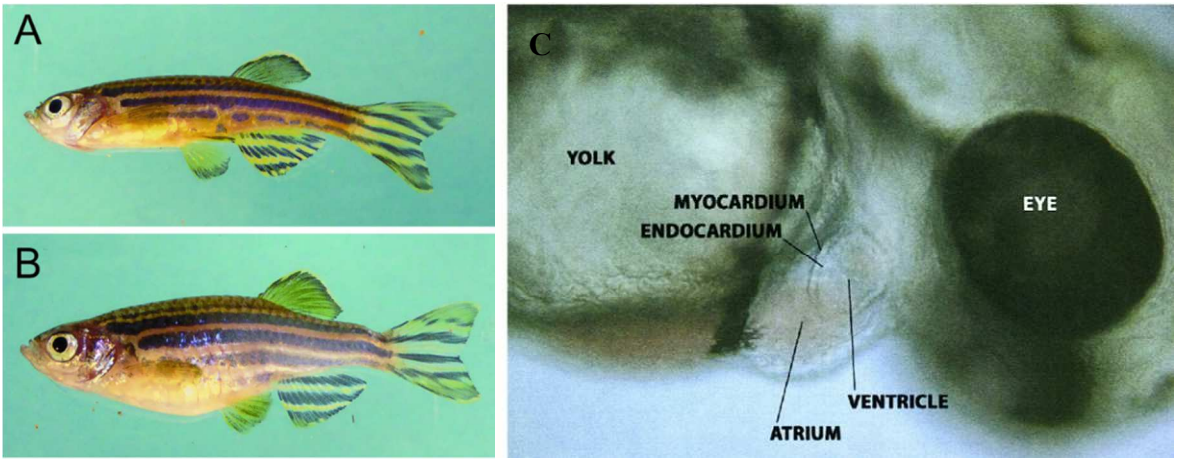

Figure 1.1 –Adult wildtype zebrafish used as model organism. A- Male zebrafish. B-Female zebrafish. C- Lateral view of a 2□day□old (48-hour post fertilization) zebrafish embryo; anterior to the right in C. The heart is located posterior to the head and anterior to the yolk. The ventricle is in focus, and its myocardial and endocardial layers are visible. (Yelon 2001, Meyers 2018)

Zebrafish genome and resemblance to human:

The parallels between particular human cardiac diseases and zebrafish heart development suggest zebrafish may be profitable for deeper investigation of mechanisms that are unclear in human heart diseases (Yalcin, Amindari et al. 2017). Prior reports have demonstrated that a large number of conserved zebrafish and mammalian genes contribute in fundamentally similar ways to cardiac development (Bakkers 2011, Liu and Stainier 2012, Bournele and Beis 2016). Based on the genome sequencing data generated by Howe and his colleagues, zebrafish have approximately 26,000 total genes in their genome. It is estimated that orthologous zebrafish genes exist for at least 71.4% of human genes(Howe, Clark et al. 2013). Evolutionary analysis revealed that, due a whole genome duplication event, zebrafish frequently have more than one gene orthologous to the same gene in human (Meyer and Schartl 1999). Despite the different time periods required to complete the early processes of heart development (35 days in humans

versus 5 days in zebrafish) the cardiac system in embryonic zebrafish exhibits anatomical and physiological resemblances to human (Rocke, Lees et al. 2009, Seto, Kiat et al. 2015). The early steps of heart patterning, heart tube formation, cardiac looping, and chamber ballooning in zebrafish are quite comparable to the mammalian heart, although later steps such as atrial and ventricular septation that create the four mammalian cardiac chambers do not occur in the fish. The human fetus at 3-weeks gestation and zebrafish embryo at 2 days post-fertilization share a similar design of the heart chambers (Baker, Warren et al. 1997). The embryonic zebrafish conduction system that functions as a key to initiate and maintain the rhythmic heartbeat resembles that of the human heart, in particular with regard to the activity and function of pacemaker cells in the sinoatrial node (Chi, Shaw et al. 2008, Poon and Brand 2013, Bournele and Beis 2016, Poon, Liebling et al. 2016). These striking resemblances of the embryonic zebrafish cardiovascular system with humans enables the study of molecular and cellular mechanisms involved in human cardiovascular diseases such as congenital heart defects, arrhythmia and cardiomyopathy (Figure 1.2)(Nemtsas, Wettwer et al. 2010, Asnani and Peterson 2014).

Zebrafish models related to cardiac disease:

Another special feature in the process of zebrafish heart development enables a direct noninvasive investigation in the cardiovascular research: Embryos in the first developmental week do not depend on the heart for oxygen delivery. Rather, adequate oxygen for survival can be obtained by passive diffusion from the surrounding aqueous medium through the skin of the larvae until approximately seven days post-fertilization (Pelster and Burggren 1996, Sehnert, Huq et al. 2002). This serendipitous trait permits researchers to examine defects in the cardiovascular system in young embryos without the complications of hypoxia. Moreover,

embryos with genetics that produce a severely malformed heart can nevertheless survive and be studied during early embryogenesis (Steed, Boselli et al. 2016). In contrast, neither avian nor mammalian embryos could live in absence of a beating heart from the earliest stages of development onward. Taken together, these advantages in zebrafish support investigations of the effects of mutant genes upon heart morphology and function, and the modeling of mutations that in humans lead to severe congenital cardiovascular defects (Dahme, Katus et al. 2009, Bakkers 2011, Keßler, Just et al. 2012).

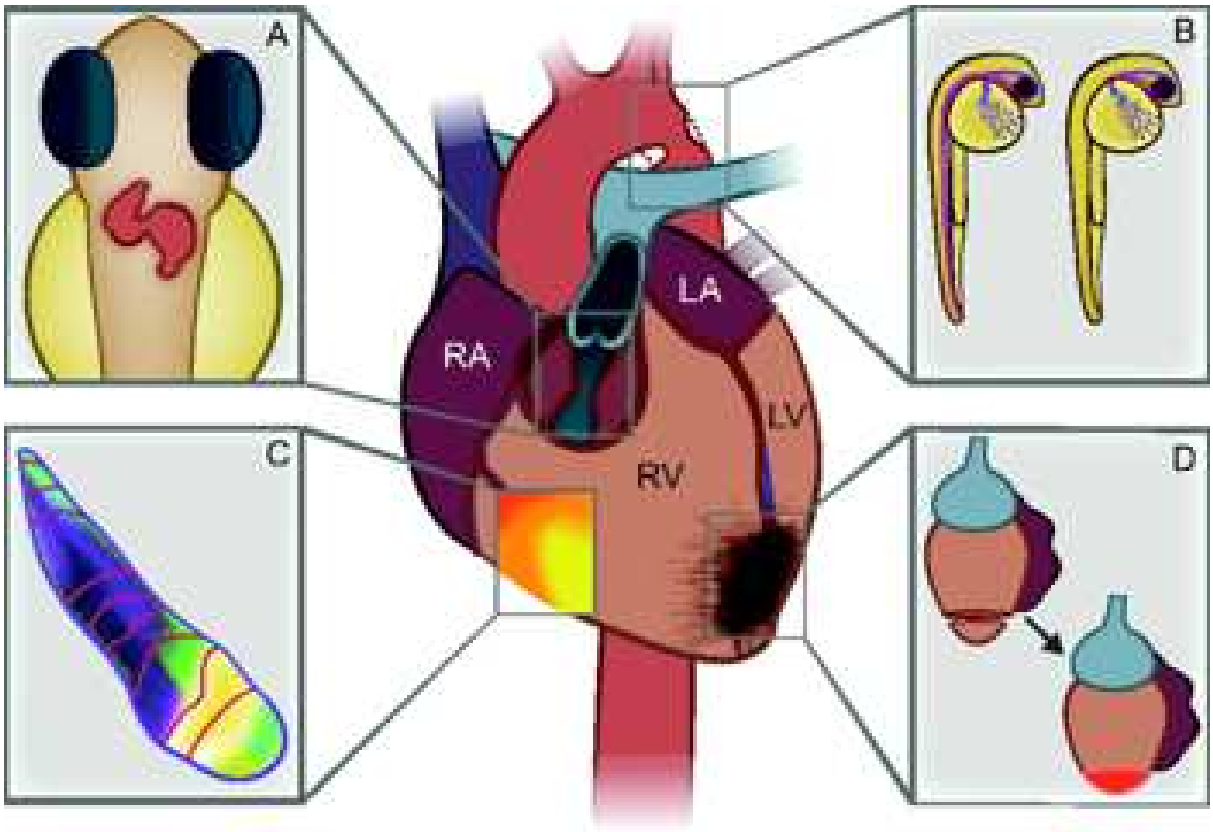

Figure 1.2– **Zebrafish models related to cardiac diseases**. The four-chambered human heart related to cardiovascular pathologies shown in middle panel .RA, right atrium; LA, left atrium; RV, right ventricle; LV, left ventricle. The examples of the development of the heart and disease studied in zebrafish is shown in side panels.
Zebrafish heart contains two chambers (atrium and ventricle). The second heart field characterization with possibility to illuminate new therapies for human congenital heart defects such as right ventricular outflow tract obstruction. (B) The *gridlock* mutation in zebrafish has defects to develop circulation in the tail and trunk (wild-type fish on left; *gridlock* fish on right) which similar to aortic coarctation in human. (C) The human heart wave propagation is mimicked by calcium activation in zebrafish and that allows the study of arrhythmias. The zebrafish isochronal mapping using a fluorescent calcium indicator (color gradient) showed calcium stimulation over time, with red lines depicting areas of the ventricle depolarized simultaneously. (D) Regeneration process in zebrafish heart. . Red cells designate regenerate of cardiomyocytes in the zebrafish(Asnani and Peterson 2014).

Zebrafish embryonic heart development:

- **The specification and differentiation of cells in the cardiogenic pools**

Formation of the zebrafish heart begins at the five hours post-fertilization (hpf) stage with specification of two different pools of progenitor cells, the atrial progenitor cells and the ventricle progenitor cells. Originally, these populations were identified by fate-mapping experiments focused on the lateral marginal zones on either side of the gastrula stage embryo (Bakkers 2011). The specification of cardiac progenitors within the anterior lateral plate mesoderm (ALPM) is accomplished by activation of several conserved genes required in the cardiac transcription program including GATA factors, Hand2, T-box proteins, and Nkx2.5 (Lu, Langenbacher et al. 2016).

- **Migration and fusion of the bilateral heart fields**

Once specified, the cardiac precursor cells migrate into the ALPM. The migration toward the embryonic mid-line is regulated by fibronectin levels, a major component of the extracellular matrix. The role of fibronecting in this process is supported by mutations in fibronectin that cause cardia bifida, a condition in which two bilaterally located heart tubes arise (Matsui, Raya et al. 2007, Staudt and Stainier 2012).After the migration of cardiac precursor cells ,, the specified progenitors continued differentiation into ventricular and atrial cardiomyocytes although they are physically separated,. Each of these sub-pools expresses chamber-specific cardiac genes such as ventricular myosin heavy chain (*vmhc*) and myosin heavy chain 6 (*myh6)* beginning around 16 hpf (Tu and Chi 2012). From 18-21 hpf, the bilateral heart fields meet and fuse at the embryonic midline, creating a cardiac cone. Within this ring/cone organization, the endocardial cells are located in the inner circular region surrounding a lumen, ventricular cardiomyocytes are found at the circumference outside of the endocardium, and atrial cardiomyocytes are found at the outermost periphery.

- **Formation of the linear heart**

Around 21 hpf, the cardiac cone begins to transition into a linear heart tube via the elongation of cardiac cone anteriorly (Chi, Shaw et al. 2008, Yalcin, Amindari et al. 2017). Once formed, the linear heart tube is composed of an outer muscular layer that contains contractile myocytes, and an inner endothelial layer comprised of endocardial cells (Stainier 2001). An elastic extracellular matrix layer known as cardiac jelly separates these two layers. Around 24 hpf, the first contractions of the linear heart tube initiate at the venous pole and contraction progresses along the tube in a rhythmic peristaltic-like manner (Andrés-Delgado and Mercader 2016). At 28 hpf, additional cardiac cells migrate into the heart tube in a second wave of differentiation to create the second heart field (SHF). In mammals, SHF cells give rise to the right ventricle, the outflow tract and part of the atria (Hami, Grimes et al. 2011). Zebrafish SHF cells give rise to the outflow tract, right ventricle, and much of the atria(Knight and Yelon 2016). The formation of linear heart tube is complete when the venous pole is displaced to the anterior left and the arterial pole is aligned with the body midline (Bakkers 2011).

- **Cardiac looping and the conduction system**

At 33 hpf, the heart begins a morphogenic process termed cardiac looping in which the linear heart tube assumes an S-shape. As a result of cardiac looping, the ventricle acquires an anterior position and the atrium becomes positioned posteriorly (Bakkers 2011). Function of the cardiac conduction system begins around 36 hpf, and is accompanied by the conversion of pumping mechanisms from slow peristaltic waves into sequential chamber contractions (Yalcin, Amindari et al. 2017).

- **Atrioventricular valve formation**

The atrioventricular canal (AVC) forms between the atrium and ventricle, beginning around 30 hpf. Valve morphogenesis at the AVC initiates with cell shape changes in AV myocardial cells,

which broaden their basolateral surface while constricting their apical (lumen-facing) surface. This process starts around 36 hpf and is completed by 55 hpf (Beis, Bartman et al. 2005). The differentiation of AVC myocardium is associated with molecular changes that parallel the morphological changes in the AV endocardial cells. At 37 hpf, the initially broad myocardial expression of *bmp4*, *tbx2b*, and *versican* throughout the heart becomes restricted to the atrioventricular myocardium, suggesting further specification has occurred in the AVC at the molecular level (Walsh and Stainier 2001). By ~45 hpf, the initially broad endocardial expression of *notch1b*, *hyaluronan synthase* 2 and *neuregulin* becomes restricted to the AV endocardium (Chi, Shaw et al. 2008). As AV canal endocardial cells undergo cellular change from squamous to cuboidal, they start expressing *Dm-grasp* (also known as *ALCAM, activated leukocyte cell adhesion molecule*), a cell adhesion molecule (Chi, Shaw et al. 2008, Scherz, Huisken et al. 2008). The onset of *Dm-grasp* expression is used in our study and others to signify the differentiation of AV endocardial cells at 36 hpf, but note this gene is also broadly expressed in the myocardium during this time.

- **The formation of endocardial cushions**

By 2 dpf, the endocardial cushions arise at the AVC, derived from the endothelial layer of the heart. The endocardial cushions are a transient structure generated by the increase of the cardiac jelly, a specialized extracellular matrix (ECM) located between the endocardium and myocardium at the AV canal (Beis, Bartman et al. 2005). By 3 dpf, endocardial cells will have remodeled into valve leaflets and folded into the cardiac jelly (Yalcin, Amindari et al. 2017). Formation of atrioventricular valve leaflets begins around 60 hpf when the atrioventricular endocardial cells undergo an endothelial-to-mesenchymal transition (EMT) and begin their folding into the thickened AVC cardiac jelly (Beis, Bartman et al. 2005, Scherz, Huisken et al.

2008). Before 76 hpf, endocardial cushions within the AV canal are not sufficient to completely prevent retrograde blood flow. As a result, normal hearts exhibit a limited amount of reverse flow, in which blood cells move from the ventricle back into the atrium during ventricular systole. Once the leaflets form, reverse flow is ablished. The heart at 48 hpf has a sinus venosus where blood enters the heart and where pacemaker cells are located. It has two chambers, including a single atrium that receives deoxygenated blood and contracts to drive it into the single ventricle, which subsequently contracts strongly to deliver blood to the body through the aorta (Yalcin, Amindari et al. 2017). After 48 hpf, the outflow tract (where blood leaves the heart to return to circulation) transitions to a pear-shaped chamber (termed the bulbus arteriosus) which accumulates blood briefly as it leaves the ventricle and functions to provide a more consistent blood flow throughout the body (Grimes, Stadt et al. 2006).

- **The formation of mature valves**

High-speed imaging studies illustrate that by 72 hpf, any reverse blood flow is totally blocked by the construction of primitive valve leaflets that align together to close off the AVC lumen during ventricular contraction (Scherz, Huisken et al. 2008, Lindsey, Butcher et al. 2014). Recently, Gunawan and colleagues demonstrated that the formation of the superior valve leaflet at 55hpf, defined as the region of the AV canal next to the inner curvature of the ventricle, precedes formation of the other valve leaflet (inferior), defined as the region next to the out curvature of the ventricle(Gunawan, Gentile et al. 2019). Notably, the superior valve leaflet was shown to be able to prevent retrograde flow independently from the inferior valve leaflet at 77 hpf (Gunawan, Gentile et al. 2019). However, at late larva stage (77 hpf) the authors hypothesized that the development of inferior valve leaflet is critical to ensure unidirectional flow (Beis, Bartman et al. 2005, Gunawan, Gentile et al. 2019). By 85 hpf, the AV endocardial cells have divided to form

two cell layers, with the endocardial cells nearest to the AV canal maintaining their cuboidal shape while those closest to the chambered myocardium changing to a rounder shape (Tu and Chi 2012). By 96 hpf, these primitive valve leaflets further differentiate into mature valve leaflets (Beis, Bartman et al. 2005, Scherz, Huisken et al. 2008). The zebrafish heart ultimately forms two sets of valves. The first (forming earliest, and studied in our work) is located in the AV canal between atrium and ventricle as just described. A second valve forms in the outflow track between the ventricle and bulbus arteriosus (Yalcin, Amindari et al. 2017).

Biomechanical factors and mechanical forces in cardiac development

Recent findings in the study of valve morphogenesis determined that biomechanical factors related to heart contraction and blood flow critically modulate the differentiation process. In this context, endocardial cells serve both as a sensor and signal transducer of biophysical forces that communicate to the cell nuclei in both endocardial and myocardial cells. Mechanotransduction is defined as the cellular processes of converting mechanical stimuli into biochemical, and genetic responses. Mechanotransduction can highly be sensitive to the forces generated during contraction itself, as well as shear stress generated by hemodynamic factors (blood flow)(Miyasaka, Kida et al. 2011).

- **Mechanical forces and shear stress**

It is increasingly appreciated that several developmental and maturational processes of the heart require mechanical forces (Petridou, Spiro et al. 2017, Schiffhauer and Robinson 2017). Mechanical forces regulate cell behavior including differentiation, cell proliferation and tissue morphogenesis. Cells must translate the physical stimuli from their local environment into biochemical signals that generate the cells' proportional response to mechanical forces. For

instance, the contractility of the heart generates mechanical forces that are essential for cardiomyocyte maturation (Fukuda, Gunawan et al. 2019). Cardiomyocytes exhibit nascent myofilaments in the early cardiac stages (22 hpf) which then develop to form sarcomeres, the contractile unit of the muscles (Reischauer, Arnaout et al. 2014, Yang, Schmidt et al. 2016). A recent study in zebrafish heart investigated the process of how intercellular mechanical forces regulate myofilament maturation through the VCL-SSH1-CFL axis, as defined below (Fukuda, Gunawan et al. 2019). Cardiac contractility regulates the localization and activation of a mechanosensitive factor known as cytoskeletal protein vinculin (VCL). VCL is an adapter molecule that functions by linking adhesion complexes to actin filaments that stabilize cell extracellular matrix adhesions or cell-cell junctions. The role of VCL is to recruit the Slingshot protein phosphatase (SSH1) which, in turn, leads to activation of its downstream effector Cofilin (CFL), an actin depolymerizing factor. These events regulate f-actin rearrangement and promote cardiomyocyte myofilament maturation (Atherton, Stutchbury et al. 2016). Taken together, these findings demonstrate that cardiomyocyte myofilament organization and growth are regulated by the transduction of mechanical forces into biological signals (Fukuda, Gunawan et al. 2019).

A second important biomechanical signal is shear stress. Shear stress can be considered a type of friction exerted by blood cells on the epithelial and endocardial lumen as they flow through the heart. Remarkably, even the direction (retrograde flow, forward flow or oscillatory flow) of blood seems to exert separable forces in zebrafish AVC development. Shear stress-related biomechanical factors specifically modulate the function of endocardial cells within the normal developing heart by activating mechanosensors that produce changes in signaling pathways leading to change in gene expression and protein function (Chien 2007). Within the AV canal, communication between the endo- and myocardium relies in part on paracrine signaling

molecules secreted in one layer that then induce changes in gene expression in the other. The Wnt and Bone Morphogenetic Protein (BMP) pathways are examples of critical paracrine signals used in early valve development (Hurlstone, Haramis et al. 2003, Chi, Shaw et al. 2008). The acute sensitivity of valve formation to biomechanical forces suggests that alteration of paracrine signals may significantly impact cell-cell communication and change the expression of genes that depend on these signals. Deciphering the mechanisms by which the endocardial cells translate the various hemodynamic forces after sensing them and defining the specific responses they produce during cardiac development are topics of intense current research (Haack and Abdelilah-Seyfried 2016).

A variety of biomechanical factors impact specific aspects of early cardiac development, ranging from chamber ballooning to ventricular trabeculation (Vermot, Forouhar et al. 2009, Boselli, Freund et al. 2015, Sidhwani and Yelon 2019). Even slight changes in the physical environment near a developing structure may induce and coordinate both local and global changes on the molecular and cellular scales (Scherz, Huisken et al. 2008, Lindsey, Butcher et al. 2014). Thus, an emerging field of research focuses on defining the complete cohort of biomechanical factors that impact various aspects of development and determining how and when the alteration of each type of biomechanical force might lead to defects in cardiac morphology or function.

The impact of biomechanical forces in zebrafish

Given that biomechanical cues by definition reflect the three dimensional environment of tissues in vivo, animal models are critical for mechanotransduction studies. Studies demonstrate that alteration the biophysical environment, such as cardiac preload, cardiac afterload, hemodynamic viscosity, and contractility in the zebrafish embryonic heart does lead to cardiac defects that resemble human congenital heart defects (Midgett and Rugonyi 2014). Zebrafish serves as an

ideal model to investigate the effects of biomechanical forces upon development of the embryonic heart since many biophysical parameters may be severely manipulated, and even stopped, without lethality, since young embryos do not depend exclusively on the oxygen carried by the blood stream.

- **Reverse flow fraction**

Critical studies from the laboratory of Scott Fraser at CalTech were instrumental in first demonstrating the specific impact of retrograde flow on valve development. The 'Reverse Flow Fraction' (RFF) is defined as the relative amount of blood that moves in the retrograde direction (from the ventricle back to the atrium) within a single cardiac cycle. Fraser's group discovered that endothelial cells located at the AV canal are exposed to dramatic hemodynamic forces that result from high velocities of blood cells moving through the narrowest region of the heart, the AVC. Moreover, alteration of hemodynamic forces resulted in malformation of the valve and associated structures. Thus, flow forces are required for normal valve morphogenesis (Vermot, Forouhar et al. 2009).

Shear stress

Shear stress is critical for chamber and valve formation. Shear stress represents the frictional forces that result from blood cell movements parallel to the vessel wall or the AVC endocardium (Chien 2007, Santhanakrishnan and Miller 2011). Shear stress represents a small fraction of total mechanical load that is sensed by the endocardium, but endocardial cells appear to be very sensitive to it. Both chick and zebrafish models suggest that alteration of the amount or duration of shear stress can lead to malformations in the developing heart (Gijsen, van der Giessen et al. 2013). Chick embryos with venous obstruction (vessel crimping to decrease blood flow into the heart) developed cardiovascular defects including malformations in the ventricular septum and

the pharyngeal arch artery. Shear stress is suggested to be involved in these defects (Hogers, DeRuiter et al. 1999, Hove, Köster et al. 2003).

In zebrafish, Hove et al altered hemodynamic flows by surgically placing an agar bead into the sinus venosus (inflow tract) to obstruct blood flow into the heart in order to test the hypothesis that blood flow influences the development of embryonic heart. Beads inserted close to sinus venosus, but which did not block flow, resulted in normal cardiac chamber and valve development, indicating that bead surgery is innocuous. In contrast, beads that were implanted in locations that did block blood flow, e.g., directly in front of the sinus venosus to block blood influx, or in the outflow tract to block blood efflux, effectively produced an accumulation of erythrocytes on the yolk or in the cardiac chambers respectively. With the next 24 hours, these hearts demonstrated abnormal phenotypes such as the malformation or reduction of the bulbus arteriosis (outflow tract), absence of looping events, abnormal development of the inflow and outflow tracts and malformation of the AV valve (Hove, Köster et al. 2003).

Although shear stress clearly provides a required biomechanical signal(s), the molecular mechanisms and genetic basis for how it does so is only beginning to be understood. Shear stress can regulate endothelial gene expression. Recently a collection of candidate genes was identified that are affected by shear stress (Dekker, van Thienen et al. 2005). One of the best studied examples to date is the zinc finger transcription factor *krüppel-like factor 2 (klf2)*, which displays increased transcription rates in response to elevated fluid shear stress in cultured endothelial cells.

The KLF family

The Krüppel-like factors (KLFs) are a family of DNA-binding transcriptional regulators that can be found in human and many other species including *Drosophila*, mouse and chick (Nagai,

Friedman et al. 2009, Bialkowska, Yang et al. 2017). The KLF family genes have a conserved protein structure that is characterized by three conserved Cys_2/His_2 zinc-fingers in their carboxy-terminal domains, which exhibit similarity to the *Drosophila* gene Krüppel at the C-terminus. Specifically, the conserved residues comprise a GC-rich DNA-binding domain thought to mediate activation and/or repression of transcription (Nagai, Friedman et al. 2009, Oishi and Manabe 2018). In *Drosophila melanogaster* early development, the Krüppel protein functions as a morphogenic factor activated in the center of the embryo body that contributes to patterning and later segmentation of the thorax and abdomen (Nagai, Friedman et al. 2009).

In l993, KLF1 was the first member of KLFs to be identified in erythroid cells (Miller and Bieker 1993). At least seventeen mammalian KLFs have been identified since then, with various patterns of tissue distribution and functions (Fan, Lu et al. 2017). The mammalian KLFs play roles in regulation of expression of a large number of target genes. Many of these function in diverse biological processes including cell proliferation, differentiation, development and programmed cell death (Zhang, Basu et al. 2005). KLF proteins act by a common mechanism of regulation: they recruit transcriptional regulatory proteins including co-activators and co-repressors, and other chromatin remodeling proteins, to enhancer regions of DNA (McConnell and Yang 2010).

- **KLFs in development, morphogenesis, and differentiation**

The KLF proteins are highly conserved. Studies in mammals revealed that many KLFs participate in embryogenesis and fetal development (Nagai, Friedman et al. 2009). Currently, six KLFs have been linked to cardiovascular development: KLF2, 3, 4, 5, 6 and 13. By using genome-wide microarray-based gene expression analysis, Dekker and colleagues established both directly and indirectly that KLF2 regulates the expression of target genes in cultured

endothelial cells. In addition, a microarray analyses revealed that a number of genes controlled by fluid shear stress required KLF2 induction (Dekker, Boon et al. 2006). In support of the cell culture experiments, several studies in fish, chick, mice and humans suggest that the blood flow regulates the endothelial expression of Klf2 (Dekker, van Thienen et al. 2005, Groenendijk, Hierck et al. 2005, Parmar, Larman et al. 2006).

During mouse embryogenesis, vascular endothelial cells robust express KLF2 between E9.5 and E12.5. A study by Lee and colleagues demonstrated that mouse KLF2$^{-/-}$ embryos developed defects in the heart ultimately leading to fetal death due to a loss of peripheral vascular resistance and defective endothelial cell function (Lee, Yu et al. 2006). In chick, Groenendijk and colleagues illustrated that a venous clip procedure designed to disrupt cardiac blood flow patterns and increase shear stress, created changes that were accompanied by alteration of gene expression patterns for KLF2 as well as other shear stress-related genes (Groenendijk, Hierck et al. 2005).

The mouse and chick KLF2 gene shares 5 blocks of conserved sequence within the N-termini with zebrafish Klf2a, Klf2b and Klf4 (Oates, Pratt et al. 2001). In all, the zebrafish genome encodes no fewer than 22 Krüppel-like factors (ZFIN.org). This large gene family has potential roles in several processes during development, including hematopoiesis, blood vessel function, and fin and epidermal development.

- **Zebrafish Klf2a and Klf2b**

The zebrafish *klf2a* and *klf2b* genes were identified by sequence alignment to be co-orthologs of mammalian KLF2 gene (Oates, Pratt et al. 2001). In zebrafish, Klf2a encodes a protein with 347 amino acids, whereas the Klf2b and Klf4 proteins have 363 and 409 amino acids respectively. From *in situ* hybridization experiments to examine the expression patterns of the two paralogous

genes, Oates and colleagues reported that *klf2a* and *klf2b* are both genes are expressed at the gastrula stage in the ventral ectoderm and *klf2a* is expressed later in the forming blood vessels or in the epidermis (Oates, Pratt et al. 2001). Molly Zeller, a previous member of our group used RT-PCR, a more sensitive technique, to demonstrate that all three genes are expressed from 5 - 72 hpf, which represents a critical window of heart development in embryonic zebrafish (Figure 1.3)(Zeller 2015). Cardiac expression of all three genes continues at 24, 36, 48, 56, 72, and 96 hours post fertilization – that is, during the entire embryonic window of heart development. In particular, expression in the AVJ region was observed for *klf2a* and *klf2b* (Zeller 2015).

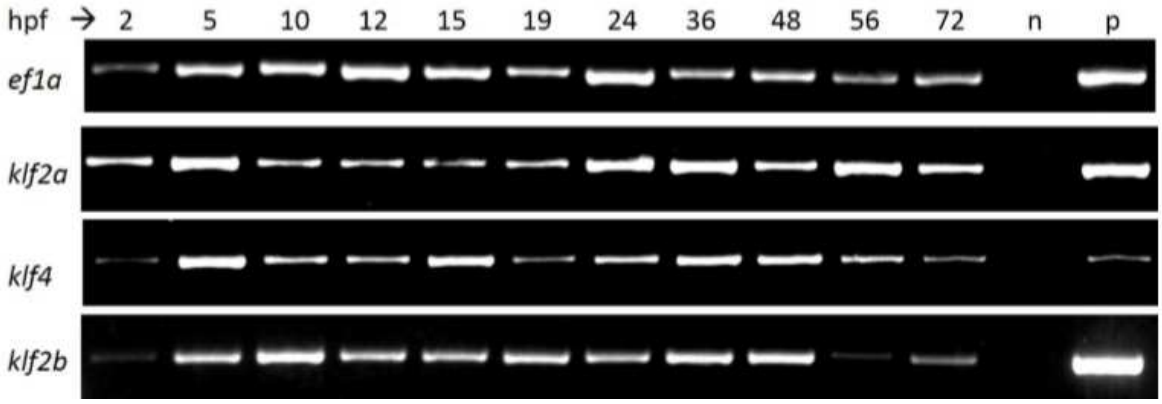

Figure 1.3– **KLF2a, KLF2b and KLF4 expression level in early development.** RT-PCR of whole embryo using gene-specific primers. *KLF2A, KLF2b* and *KLF4* are express from two hpf to 72 hpf. The positive control isthe elongation factor 1α(ef1α)(Zeller 2015).

- **Importance of *klf2a* for atrioventricular valve development**

klf2a is a flow-responsive gene that demonstrates its highest level of cardiac expression in the atrioventricular canal (AVC)(Vermot, Forouhar et al. 2009). *klf2a* plays a fundamental role in valve formation and the endocardial cell surface area (Vermot, Forouhar et al. 2009, Dietrich, Lombardo et al. 2014). The landmark study by Vermot and collleagues (2009), demonstrated that *klf2a* expression within the AVC endocardium is directly dependent on the magnitude of the

retrograde flow fraction. Analysis of *klf2a* mutant or morpholino knockdown embryos treated with drugs to reduce the reverse flow fraction showed that with reduced RFF, the AV expression of *klf2a* is absent or down-regulated, and the valve malformed (Parmar, Larman et al. 2006, Vermot, Forouhar et al. 2009).

Vermot and colleagues characterized embryonic zebrafish mutants that produced fewer or no blood cells as a means to disrupt of blood viscosity to better understand the mechanisms regulating *klf2a* transcription (Vermot, Forouhar et al. 2009). In this study, blood viscosity was altered by disruption of either *gata1* or *gata2*, two key hematopoietic transcription factors expressed during early embryogenesis and required for the embryo to produce erythrocytes (Stainier and Fishman 1994). *gata1* or *gata2* homozygous mutant embryos demonstrated significant loss in hematopoietic stem cells (and blood) but no defects in vasculature (Stainier and Fishman 1994). Likewise, morpholino knockdown of *gata2* phenocopied the significant loss of blood cells and likewise had no effects in the vascular system or body plan. Thus, *gata2* mutants represent a useful system to identify phenotypes that are associated with reduced shear stress and reduced reverse flow. The authors found that wildtype embryos normally exhibit reverse flow throughout 35% of the cardiac cycle (normal RFF=35%), demonstrate normal levels *klf2a* expression at 56 hpf, and undergo normal valve development by 96 hpf. By comparison, *gata1* morphant embryos demonstrated a 90% reduction of the hematocrit levels, essentially eliminating all blood flow. Fluorescent microbeads were injected to assess RFF, which was found to be *increased* to 45%. Note that although few blood cells *per se* are present, plasma (the fluid associated with blood) remains and creates shear stress. Under these conditions, *klf2a* expression was normal in 78% of embryos *klf2a* expression at 56 hpf and valve development normal by 96 hpf (Vermot, Forouhar et al. 2009). Thus, increasing RFF to 45% was usually not

harmful to AV valve development, perhaps because sufficient shear stress occured. On the other hand, RFF in *gata2* morphant embryos hematocrit levels were *decreased* to 17%. This condition maintained a low amount of blood flow without eliminating it entirely, but shear stress was reduced relative to wildtype. *klf2a* expression at 56 hpf was 5-fold lower than controls, and only 36% of embryos exhibited normal valve development by 96 hpf. These data revealed that valve dysgenesis is linked to reduced RFF and reduced shear stress. To confirm the connection between reduction of RFF and valve dysgenesis, double *gata* knockdown embryos were examined (Vermot, Forouhar et al. 2009). Simultaneous injection of *gata1* and *gata2* morpholinos produced embryos that resembled *gata1* knockdown in that very few blood cells were produced. The RFF of 50%, quite similar *gata1* knockdown (45%). Like *gata1* morphants, valve formation was normal in 87% of embryos. Altogether, these results indicated that maintaining a certain minimal amount of RFF is a critical factor for normal valve development (Vermot, Forouhar et al. 2009).

klf2a is hypothesized to act downstream of blood flow-induced biomechanical factors, and is transcriptionally responsive to these forces (Vermot, Forouhar et al. 2009). In homozygous mutants for *troponin2* (*silent heart, sih* mutants), which completely lack cardiac contraction and therefore exhibit no blood flow (or plasma flow) at all, *klf2a* expression was downregulated or absent and there is an increase in valve dysgenesis (Parmar, Larman et al. 2006, Vermot, Forouhar et al. 2009). Knockdown of *klf2a* via morpholino produced embryos with normal cardiac contractility and normal blood flow at 48 hpf (Dietrich, Lombardo et al. 2014), consistent with the hypothesis that this gene acts downstream of shear stress-related factors. However, at 96 hpf, AV valve function was decreased in 72% in the *sih* embryos (Vermot, Forouhar et al. 2009), consistent with the idea that normal blood flow and shear stress were

present, but the key Klf2a-mediated mechanotransducer pathway was nonfunctional (Vermot, Forouhar et al. 2009).

In response to shear stress signals, Klf2a was hypothesized to regulate endocardial cell size. Dietrich and colleagues found support for this hypothesis by overexpression of *klf2a,* which led to a reduction in endocardial cell size (Dietrich, Lombardo et al. 2014). Collectively, these data showed that the expression of the gene *klf2a* depends on the existence of reverse flow (shear stress) and is essential for valve development.

A previous study showed that *klf2b,* the paralog of klf2a, is not responsive to changes in blood viscosity or cardiac contractility (Zeller 2015). *Klf2b* is expressed in the central mesenchyme of the pectoral fin bud and in the adjacent cleithrum of the shoulder girdle (Yokoi, Yan et al. 2009). Expression of *klf2b* occurs in ectoderm, neural crest, and periderm in early embryonic stages from 50% epiboly to 20-25 somites, but no expression was reported later than 48hpf (Thisse, Pflumio et al. 2001). Given the degree of amino acid similarity, Klf2b may function redundancy with Klf2a. Molly Zeller examined the expression of *klf2b* in the heart via RT-PCR, illustrating that *klf2b* was expressed in the heart from 36 to 96 hpf. Moreover, *klf2b* expression was restricted to the ventricle and AVJ from 48 to 96 hpf (Zeller 2015). Thus, Klf2b is not essential for the early embryonic development, but it could contribute to the later stages of heart development (Zeller 2015).

- **Zebrafish Klf4**

In zebrafish, *klf4* is expressed in the hatching gland, lateral line ganglia, neuromasts, and blood (Thisse and Thisse 2004). Molly Zeller's RT-PCR studies showed that *klf4* is expressed in heart from heart tube to valve formation stage (96 hpf)(Zeller 2015). Its expression occurs prior to expression of several genes required for hematopoiesis, including *gata2*, *pu.1*, and *scl*/*tal-1*.

Thus, it is possible that Klf4 regulates erythropoiesis and myelopoiesis since it may act upstream of these transcription factors. The depletion of *klf4* by morpholino generated defects in hemoglobinisation of the red blood cells, anemia, pericardial edema, and hatching defects (Oates, Pratt et al. 2001, Gardiner, Gongora et al. 2007), suggesting *klf4* plays critical roles in embryonic globin and heme synthesis as well as hatching gland gene expression. However, *klf4* is not significantly altered by changes in blood viscosity or cardiac contractility (Zeller 2015), indicating it is not a flow responsive gene.

***Filamin C* gene:**

Filamin C (*FLNC*) is a dimeric actin crosslinking protein that acts as a scaffold for many cytoskeletal structural and signaling proteins (Bournele and Beis 2016). The human *FLNC* gene is duplicated in the zebrafish genome, creating two paralogs (*flnca* and *flncb*) that both share high amino acid identity to human *FLNC* (~79 to 82% amino acid identity)(Begay, Tharp et al. 2016). Vertebrate *FLNC* is highly expressed in the skeletal and cardiac muscles. At 2,773 amino acids, it is one of the largest proteins to localize to the Z-disc (Begay, Graw et al. 2018).

- **FLNC structure**

The structure of Filamin proteins is highly conserved among vertebrates; typically the N-terminus consists of two calponin homology (CH) domains that contain actin binding sites in the N- terminus. Following these domains, filamin proteins exhibit 24 immunoglobulin-like domains that extend over 80% of the protein, with the final (24th) Ig-like domain mediating formation of homodimers (Sanoja, Li et al. 2018). The 19th through 24th Ig-like domains also contain the binding sites for several of the FLNC interacting proteins, including xin, migfilin, myotilin, integrin β1A, FATZ-1 and γ- and δ-sarcoglycan (Fujita, Mitsuhashi et al. 2012).

- **Biological function**

The sub-cellular location of vertebrate FLNC in the Z-disc, costamere and intercalated disc/myotendinous junction are consistent with structural functions in each context. Within the Z-disc, *FLNC* interacts with multiple Z-disc proteins such as myotilin and myopodin(van der Ven, Wiesner et al. 2000, Linnemann, van der Ven et al. 2010). Early immunohistochemistry experiments on cultured skeletal myotubes stimulated to differentiate as muscle cells showed that FLNC co-localized with α-actinin in the forming Z discs (van der Ven, Obermann et al. 2000). The timing and subcellular location of Flnc protein suggested its possible contribution to the early stages of sarcomerogenesis including the formation of the Z-disc and myofibril (Fürst, Goldfarb et al. 2013). Indeed, recent data from our lab support this hypothesis. FLNC knockdown by siRNA in the mouse myoblast cell line C2C12 caused differentiation defects that reduced the ability of myoblasts to fuse, and eliminated their ability to for myotubes. These data support a role for FLNC in myogenesis well before the onset of sarcomere formation (Dalkilic, Schienda et al. 2006). A mouse model of FLNC (discussed further below) showed severe defects in skeletal muscle that lead to death immediately after birth, due to the failure of respiratory muscles to move the diaphragm (Dalkilic, Schienda et al. 2006). Hearts of homozygous mice appeared normal so far as they were investigated.

Within the costamere, low amounts of *FLNC* are observed in cytoplasm near the sarcolemma. Through its association with over 90 proteins in the cortical cytoplasm, FLNC connects the sarcolemma, cytoskeleton and myofibrils (van der Flier and Sonnenberg 2001). As an actin-binding protein, FLNC plays an important role in actin organization and cytoskeletal stabilization (Chakarova, Wehnert et al. 2000). In the costamere, FLNC interacts with transmembrane proteins, including the receptor β1-integrin and γ- and δ-sarcoglycan (Figure 1.4)

(Thompson, Chan et al. 2000). FLNC linkage to protein complexes within the sarcolemma connects the internal cytoskeleton with the extracellular matrix (Thompson, Chan et al. 2000, van der Ven, Obermann et al. 2000). The cross-linking abilities of actin-binding proteins like FLNC facilitate structural strength and physical integrity within the cell, thus serving a mechanoprotective function. Filamin proteins are not permanently wedged within the cytoskeletal network, but rather have a surprising ability to dynamically relocate within the cell. In fibroblasts, filamin A can be recruited to integrin complexes in the cell membrane in response to stress or force application to the ECM. Filamin A relocation triggers a cytoplasmic rearrangement in response to the sensed tension. Cells lacking filamin A were not able to withstand force application, resulting in loss of membrane integrity and death of 90% of the cells (Thompson, Chan et al. 2000). The filamin A functions in fibroblasts suggest potential parallel functions for FLNC in the cardiomyocytes.

Finally, FLNC protein localizes to the myotendinous junctions of skeletal muscle (the site of connection between tendon and muscle) as well as the intercalated discs of cardiomyocytes (the site where individual cardiomyocytes are bonded together). Recently, knockdown of FLNC in zebrafish indicated an Flncb-mediated role in cell: cell adhesion (Begay, Graw et al. 2018).

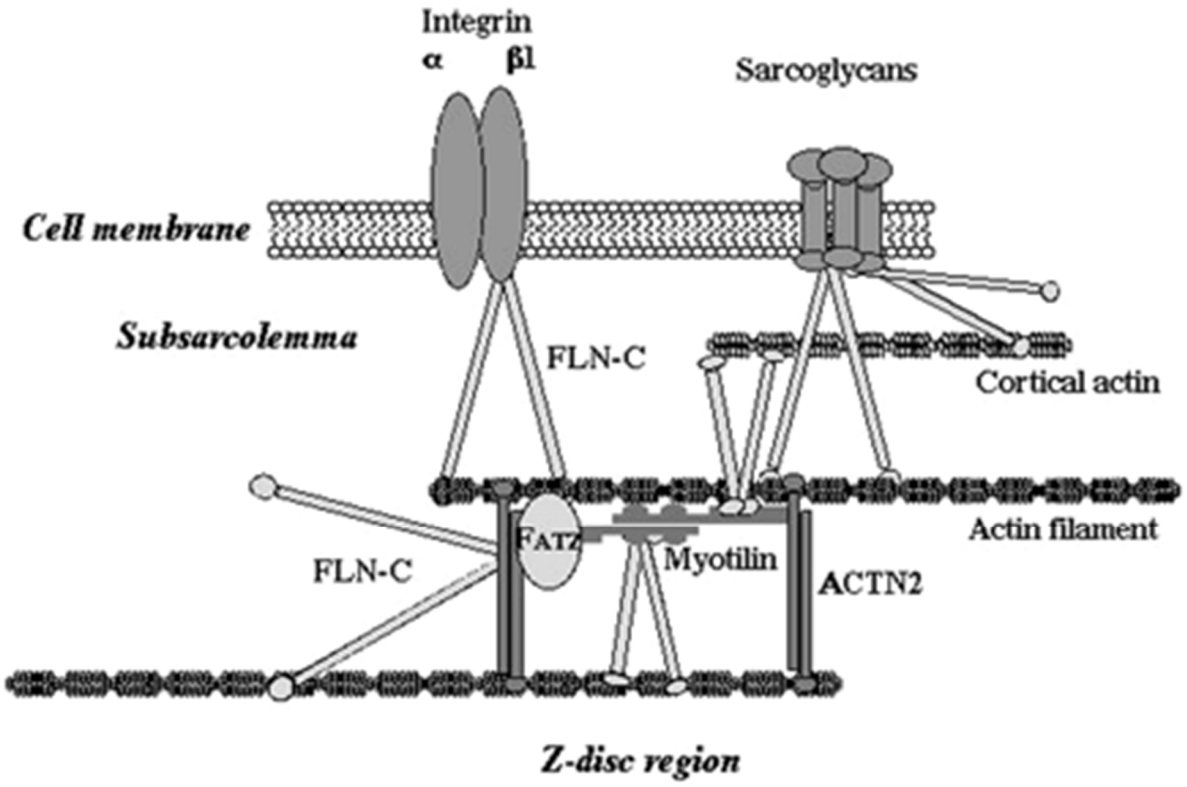

Figure 1.4– **Schematic of intracellular Filamin C localization within the costamere.** The filamin-C links cytoplasmic domain of β1 integrin and the γ and δ sarcoglycans at the sarcolemma. Also, FLNC links actin filament to sarcolemma(Groenendijk, Hierck et al. 2005).

***Filamin C* gene and myopathic disease**

- **Myofibril myopathies (MFM)**

The mutation of *FLNC* has been linked to muscle disease. The myofibril myopathies (MFM) are a group of rare human genetic disorders that target the skeletal muscle and are defined by progressive muscle weakness and physical disability (Fürst, Goldfarb et al. 2013). MFM leads to the production of intracellular protein aggregates, myofibrillar disorganization and mitochondrial defects. Pathogenic mutations associated with the MFM phenotype have been identified in 17 genes to date, most of which are associated with other muscle diseases as well (Fichna,

Maruszak et al. 2018). Several of these genes encode components associated with the Z-disc (e.g., FLNC, myotilin, and ZASP (cypher)) or components of the costamere (e.g., FLNC, desmin and plectin)(Schröder and Schoser 2009, Fichna, Maruszak et al. 2018). Clinical studies show that *FLNC* mutations are associated with muscle weakness (Luan, Hong et al. 2010, Tasca, Odgerel et al. 2012). The causative role for *FLNC* in MFM was discovered in 2005 from studies of a German family, including 8 members with a missense mutation in *FLNC* gene who showed MFM-like phenotypes (Vorgerd, van der Ven et al. 2005). Since then, at least 59 different FLNC variants, representing a range of different types of mutations, have been found to cause muscle-related disease in humans (Ader, Groote et al.)

- **Cardiomyopathy**

In recent years, mutations in human *FLNC* gene were shown to be associated with several types of cardiomyopathy including hypertrophic cardiomyopathy, dilated cardiomyopathy, arrhythmogenic dilated cardiomyopathy, left ventricle non-compacted cardiomyopathy and restricted cardiomyopathy (Ader, Groote et al.). Two patients with restrictive cardiomyopathy (RCM) were found to have missense mutations in the *FLNC* gene but did not exhibit any defects in the skeletal muscle (Brodehl, Ferrier et al. 2016). Additional studies identified many *FLNC* missense variants in families, with affected members demonstrating normal skeletal muscle fibers (based on histological and biochemical assays) but with clear evidence of hypertrophic cardiomyopathy (HCM) (Valdés-Mas, Gutiérrez-Fernández et al. 2014). A recent study defined two novel splice site mutations in the *FLNC* gene, and showed they were associated with cardiac phenotypes characterized by arrhythmia and dilated cardiomyopathy in the absence of skeletal muscle abnormalities(Begay, Tharp et al. 2016, Begay, Graw et al. 2018). Thus, MFM and cardiac disease are not always coincidental. The mechanisms underlying this variability remain

mysterious. A fascinating recent survey of 28 pathogenic FLNC variants found that all patients with DCM (13 patients) carried truncating variants (Ader, Groote et al.). All patients with HCM (11 patients) carried missense variants. Patients with other types of cardiomyopathy (4 people) carried missense or in-frame indel variants (Ader, Groote et al.). These studies seem to suggest that more than one mechanism may be at play regarding the role of *FLNC* in cardiac development, those mechanism(s) are not fully understood (Valdés-Mas, Gutiérrez-Fernández et al. 2014, Begay, Tharp et al. 2016, Brodehl, Ferrier et al. 2016). The study by Ader and colleagues further noted that HCM missense mutations were mostly found in the interaction domain between FLNC and Z-disc proteins. The authors state that all missense FLNC variants were translated. One might imagine misfolded FLNC that forms aggregates or sequesters vital binding partners. In contrast, the authors claim (but do not actually show) that patients with DCM encode FLNC truncating variants, but none of them are translated. Ruparelia and colleagues developed zebrafish models to explore the pathophysiology of these truncating variants. Haploinsufficiency (or loss of function) seems the most likely mechanism here (Ader, Groote et al.).

Animal model to study *FLNC* function:

- **Mouse**

Animal models have been used to investigate the role and function of *FLNC* in embryos that exhibit MFM or cardiomyopathy phenotypes (Figure 1.5). A spontaneous *FLNC* mouse mutant was discovered in which the last eight exons out of 48 total in the *FLNC* gene were deleted. This mutant parallel a *FLNC* truncation mutation that causes a partial loss of function phenotype in human patients (Dalkilic, Schienda et al. 2006). Mutant mice showed severe skeletal muscle defects and died soon after birth due to a weakened ability of muscle required to breath. Neonatal

homozygous mice did not exhibit cardiac defects in this model. Thus, this model is not suitable for study of the early developmental phenotypes leading to cardiomyopathy (Dalkilic, Schienda et al. 2006).

- **Medaka**

Another animal model used to study the role of *FLNC* mechanism in cardio and skeletal muscle development is medaka (*Oryzias latipes*) (Fujita, Mitsuhashi et al. 2012). In this model, one of two paralogous *FLNC* genes (*FLNCa*) harbors a nonsense mutation suggested to encode a truncated protein in the 15th immunoglobulin-like repeat. These mutant fish are named *zacro* (*zac*). In medaka, *FLNCa* is expressed in both skeletal and cardiac muscle. (The expression of *FLNCb* in medaka was not investigated in this study.) Homozygous *zac/flnca* embryos presented skeletal muscle defects due to myofibril disruption and disorganization. Cardiac abnormalities were detected in homozygous *zac* mutants; specifically, the myocardial layer of the heart ruptures near the onset of regular cardiac contraction. In *zac* embryos, the myofibrils were disconnected from the sarcolemma and intercalated disks. Morpholino studies yielded phenotypes similar to the *zac* mutants. Overall, the medaka *FLNCa* mutant model supports a critical role for *FLNC* in maintaining the structural integrity of cardiac and skeletal muscles (Fujita, Mitsuhashi et al. 2012).

- **Zebrafish**

Additional models are needed to understand the wholistic *FLNC* function in the heart, to determine whether the *flnca* and *flncb* genes are functionally redundant, and to investigate the mechanisms that cause cardiac or muscle diseases. The zebrafish *Danio rerio* are the ideal model to study human heart disease since this model system has special characteristics that do not exist in other models, including the ability to study the cardiac development in embryos with severe

cardiac defects. The *FLNC* gene is represented in zebrafish by two paralogs, *flnca* and *flncb,* which are 80% and 84 % identical to human *FLNC* at the amino acid level respectively (Begay, Tharp et al. 2016).

***FLNC* gene and skeletal muscle phenotypes:**

The *stretched-out (sot)* mutant is the first-described zebrafish *flncb* mutant (Ruparelia, Zhao et al. 2012). Ruparelia and colleagues identified *sot* mutants in a genetic screen, and examined them as a novel zebrafish model of filamin-related MFM to understand the roles of *FLNC* in muscle development and function. *sot* fish carry a *flncb* nonsense mutation that encodes a premature stop codon at exon 30 (c.5056A>T; ENSDART00000026492) out of 49 exons. (The naming of Flnc exons includes 40 and 40a, so the final exon carries the number 48, not 49)(Chakarova, Wehnert et al. 2000). Homozygous *sot* mutants displayed mild skeletal phenotypes including sporadic disintegration of the skeletal slow muscle fibers and the accumulation of protein aggregates containing myosin and desmin. The aggregates tended to be large, globular, and located near the myosepta. Both skeletal muscle wasting phenotypes and protein aggregation are considered hallmarks of human MFM disease (Ruparelia, Zhao et al. 2012). Intriguingly, these phenotypes were evident in homozygous *sot* embryos only between the 24-somite and 32-somite stages, whereas in later stages the slow muscle fibers were completely normal. These authors further demonstrate that using morpholinos to deplete both *FLNC* homologues (*FLNCb* and *FLNCa*) led to much more catastrophic skeletal muscle degeneration phenotypes. Therefore, these studies provide evidence for *FLNC* functional redundancy in fish skeletal muscle. These studies did not address heart development since skeletal muscle phenotypes were the main investigation. Additionally, it is not clear whether the potential

truncated protein is indeed translated and whether it is partially functional or undergoes nonsense-mediated decay and represents a full loss of function (Ruparelia, Zhao et al. 2012).

***FLNC* gene and cardiac phenotypes:**

In collaboration with investigators at UC Anschulz, our group developed the first animal model for study of the *FLNC* contribution to cardiac phenotypes (Begay, Tharp et al. 2016). A need for a cardiac model was prompted by GWAS studies which discovered a novel human *FLNC* splicing variant found in three unrelated families who suffer dilated cardiomyopathy. In Begay's study, knockdown of *FLNCb* by morpholino produced severe and irreversible cardiac phenotypes in embryonic zebrafish. The heart phenotypes were associated with changes in cardiac function, increased reverse flow and reductions in cardiac contractility, stroke volume, cardiac output and heart rate (Begay, Tharp et al. 2016). Furthermore, zebrafish morphant embryos exhibited systolic dysfunction characterized by dysmorphic cardiac chambers, pericardial edema, and looping defects at 48 and 72 hpf (Begay, Tharp et al. 2016). An ultrastructural study of *FLNCb* knockdown embryos was performed to evaluate the cellular basis for the reduction in contractile function. FLNCb-depleted cardiac myofibrils consisted of a low number of successive sarcomeres, and myofibrils were frequently irregular in thickness and exhibited Z-discs with irregular width, thickness, and arrangement. Given that *FLNCb* knockdown embryos produce loss-of-function effects, this study suggested a mechanism of haploinsufficiency underlies the observed cardiac phenotypes (Begay, Tharp et al. 2016). More studies are needed to investigate the mechanism by which *FLNC* mutation leads to cardiomyopathies and why different mutations of the *FLNC* gene produce a variety of cardiomyopathy types.

Given the correlations of non-translated FLNC truncating variants with DCM, and translated missense FLNC variants with HCM(Kley, Hellenbroich et al. 2007), it will be interesting to determine whether a similar correlation holds in the zebrafish model. Moreover, with the exception of our work above, all prior animal models, and the large majority of human cellular analysis has focused on the effects of FLNC mutations skeletal muscle. Although parallel cell-based phenotypes are likely to be found in the developing heart, it is yet to be shown whether FLNC depletion phenotypes have analogous outcomes for Z-disc, costamere and intercalated disc function, and whether aggregates form in the same location or with the same components.

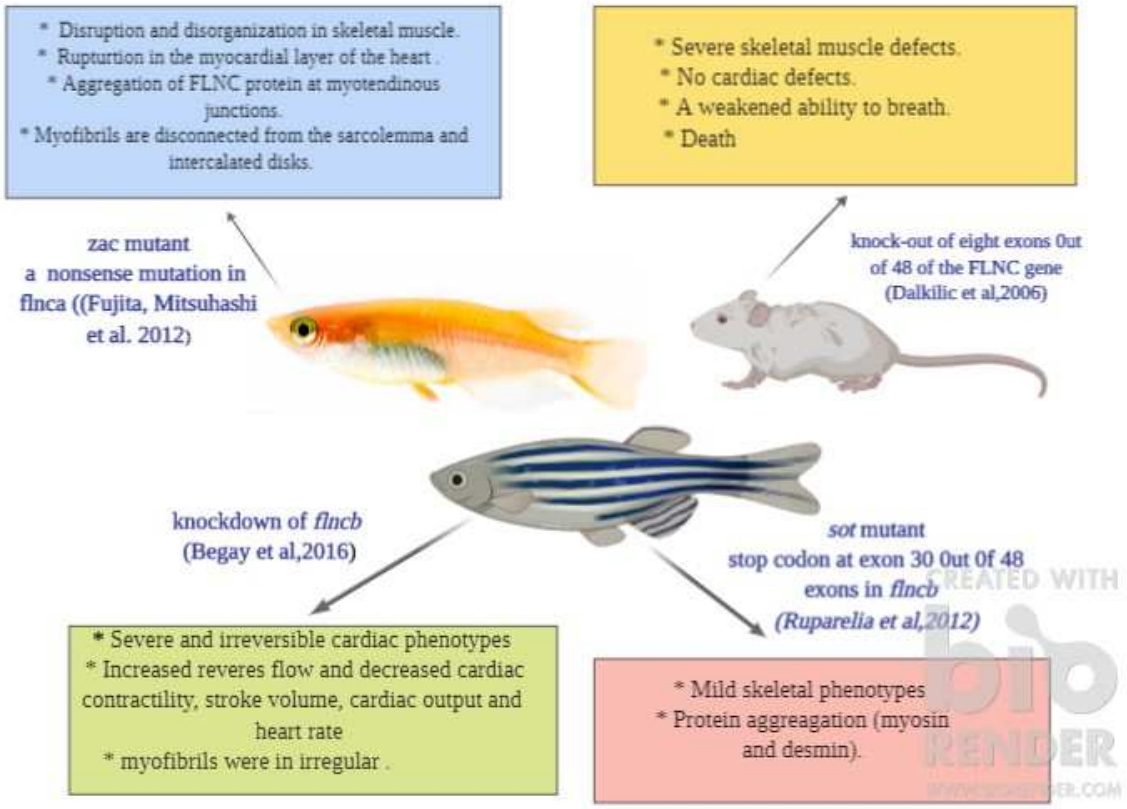

Figure 1.**5 - Overview of animal models used for modeling *the role and function of FLNC***

Our group has extensively developed the zebrafish model to investigate the contributions of various *flnc* alleles leading to cardiac muscle disease. For her PhD dissertation, Rasha Alnefaie

completed a study of duel loss-of-function (both *flnca* and *flncb)* using the morpholinos previously validated by Ruparelia and colleagues. Simultaneous knockdown of *flnca* and *flncb* led to abnormal heart and skeletal muscle development. The defects in the heart included disrupted cardiac morphogenesis, aberrant looping morphogenesis, reduced contractility, and altered blood flow. In the dual *flnca* / *flncb* knockdown embryos, the cardiac defects share some similarity with patients who suffer cardiomyopathy, such as altered functional performance including blood flow and low cardiac output (Begay, Tharp et al. 2016) (Alnefaie 2019). To further study the dose-dependency of *flnc*, and to examine the effects of truncation mutations in comparison to full loss-of-function alleles, Dr. Alnefaie characterized several *flnc* alleles, which are referred to here by a shorthand denoting the location of the premature stop codon. The *flcna* $^{exon\ 1\ -/-}$ and *flcnb* $^{exon\ 1\ -/-}$ alleles each contain a nonsense mutation in exon 1. If translated, these proteins would be tiny (~7 kDa compared to the wildtype ~280 kDa protein), and would be truncated within their actin binding domains. The *flcnb* $^{exon\ 14-/-}$ and *flcnb* $^{exon\ 35-/-}$ alleles encode nonsense mutations within the immunoglobulin (Ig)-like repeat regions, truncating the protein within the 4th or 17th Ig-like domain, respectively (Figure 1.5)(Alnefaie 2019). If translated, these truncated proteins would retain the actin binding domains and some of the rod domain Ig-like domains, but lack the C-terminal dimerization domain and the several C-terminal protein interaction sites found in Ig-like domains 19-24.

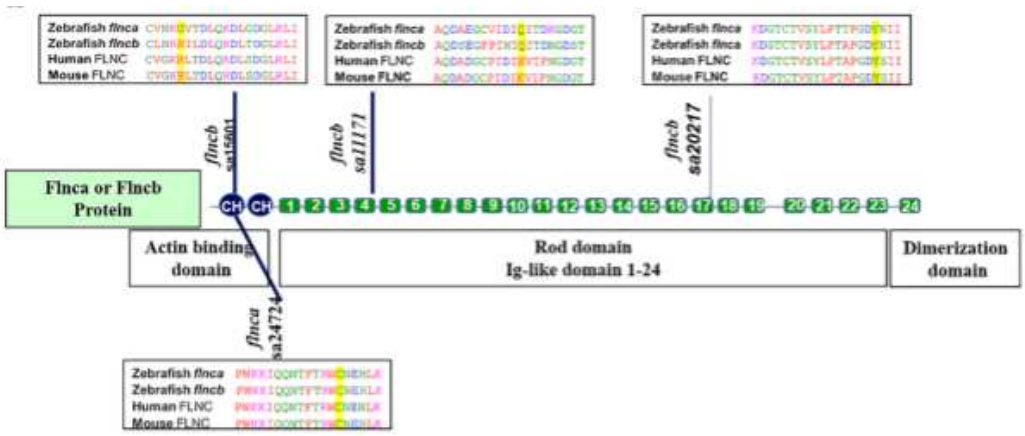

Figure 1.**5- Various alleles of *FLNC* in zebrafish.** Schematic represents the structure of *FLNC*a and *FLNC*b proteins domains, , annotated with the positions of four mutations that affect heart and skeletal muscle development. ClustalW used to generate The sequence alignment. The yellow highlighte showed the amino acids in the human and mouse *FLNC* sequences that are homologous to the zebrafish mutation sites(Alnefaie 2019).

At 24, 48, or 72 hpf, no clear heart phenotypes were observed in homozygous *flcna* $^{exon\ 1-/-}$ or *flcnb* $^{exon\ 1-/-}$ embryos. In contrast, doubly homozygous mutant (*flcna* $^{exon\ 1-/-}$; *flcnb* $^{exon\ 14-/-}$) embryos revealed abnormal “stringy” heart phenotypes and skeletal muscle myofibril phenotypes accompanied by swimming defects. Altogether, in zebrafish heart development, the *flnca* and *flncb* paralogous enact most of their functions redundantly. In fact, the single mutant *flnca* exon1 and *flncb* exon14 exhibited no significant increased looping angle. Homozygous *flncb* exon14 embryos displayed a slightly reduced heart rate, but *flnca* exon1 embryos were comparable to wildtype. Double homozygote embryos showed much stronger cardiac phenotypes including a significantly increased looping angle, significantly decreased heart rate along, decreased ventricle size, poor contractility and mild or severe cardiac edema. The cardiac phenotype seen in the double homozygote embryos was lethal.

In some but not all human patients with MFM and or cardiomyopathy, FLNC-containing protein aggregates were observed (Valdés-Mas, Gutiérrez-Fernández et al. 2014, Brodehl, Ferrier et al. 2016). Mutant FLNC proteins are altered in their ability to interact with partner proteins, or to dimerize. FLNC can accumulate in cytoplasmic aggregates, along with other Z-disc or costamere proteins(Kley, Hellenbroich et al. 2007). These aggregates may produce disease via toxic impacts on the cell (Dalkilic, Schienda et al. 2006, Ruparelia, Zhao et al. 2012). The *flcnb* $^{exon\ 14-/-}$ and *flcnb* $^{exon\ 35-/-}$ alleles encode putative truncation mutants. Rasha Alnefaie characterized scored embryos for cardiac phenotypes: cardiac edema, dysmorphic "stringy" chambers, mild edema and abnormal chamber morphology. Skeletal muscle function was scored by testing for embryo swimming defects. These phenotypes from homozygous *flcnb* $^{exon\ 14-/-}$ and *flcnb* $^{exon\ 35-/-}$ embryos were hypothesized to represent gain-of-function phenotypes since they showed more severe phenotypes than the presumed null mutant (*flcnb* $^{exon\ 1-/-}$). In conclusion, this study hypothesizes that *flcnb* $^{exon\ 14-/-}$ and *flcnb* $^{exon\ 35-/-}$ mutant animals display a gain-of-function effect which may be derived from a truncated protein that interferes with the wildtype Flnc protein, and potentially other binding proteins as well, in cardiac and skeletal muscle cells (Figure 1.6) (Alnefaie 2019).

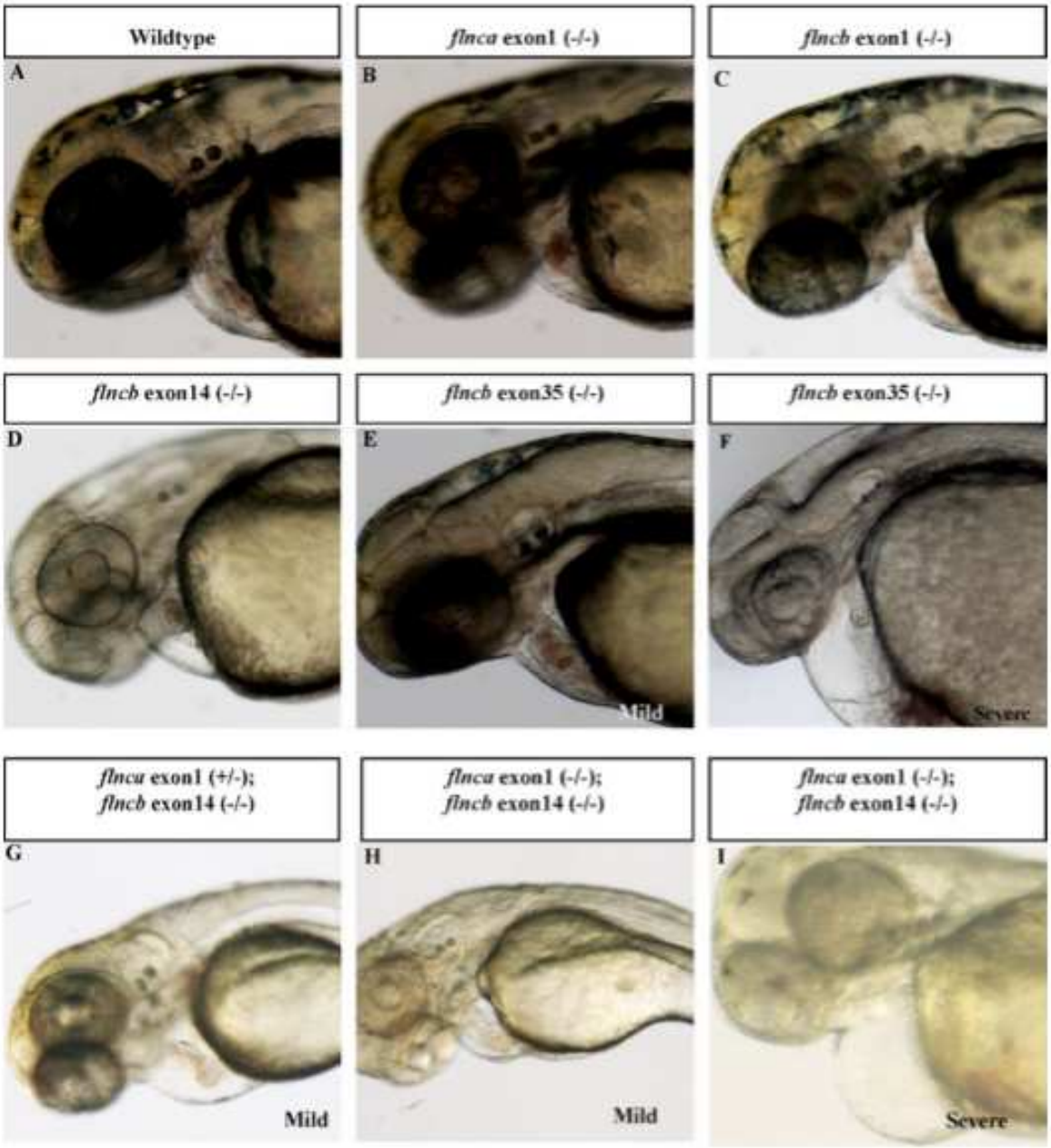

Figure 1.6- The effects of *FLNCa* and *FLNCb* alleles in the heart development. . (A-I) lateral view of zebrafish embryos at 48 hpf. (A, B, C, D) Normal heart morphology represented in wildtype and homozygous *FLNC*a exon1, *FLNC*b exon1, and *FLNC*b exon14 mutants, respectively. (E-F) homozygous *FLNC*b exon35 mutant. (E) Mildly dilated chambers. (F) Severe pericardial edema and stretched chambers. (G-H-I) double *FLNC*a exon1+*FLNC*b exon14 mutant embryos (G-H) displayed mild pericardial edema and dilated chambers. (I) Severe pericardial edema and stretched chambers.

Through studies investigating developmental aspects of Flnc depletion, Dr. Rasha Alnefaie demonstrated that Flnc (i.e., Flnca and Flncb) is required for Z-disc formation and sarcomere arrangement in cardiomyocytes of the zebrafish heart. These studies utilized the transgenic line Tg(Cmlc2: Cypher-EGFP), which marks the location of the Z-discs in the heart by expression of GFP-tagged Cypher, a Z-disc protein. At 53 hpf, the length of Z-disc (i.e., the width of one Z-disc from side to side) and the length of sarcomere (distance between two Z-discs) were measured in embryos depleted for one or both FLNC genes, either genetically or using morpholinos (MO). Tested genotypes included: wildtype, *flnca* MO, *flncb* MO, *flnca*+*bMO*, *flcna* $^{exon\ 1-/-}$ + *flncb* MO, *flcna* $^{exon\ 1-/-}$, *flcnb* $^{exon\ 14-/-}$, and double mutant *flcna* $^{exon\ 1-/-}$ + *flcnb* $^{exon\ 14-/-}$. The data indicated a significant decrease in the average Z-disc length for the *flnc*a MO, double *flcna* $^{exon\ 1-/-}$ + *flcnb* $^{exon\ 14-/}$MO, and *flcna* $^{exon\ 1-/-}$ + *flnc*b MO embryos as well as in *flcnb* $^{exon\ 14-/-}$,and double *flcna* $^{exon\ 1-/-}$ + *flcnb* $^{exon\ 14-/-}$ mutant. On the other hand, the length of the sarcomere was not significantly different among all groups expect double *flnc*a+b MOs heart which exhibited a significant increase in sarcomere length. These findings suggest that *FLNC* function is critical for Z-disc assembly(Alnefaie 2019). Moreover, at 72 hpf the sarcomere assembly in *FLNC* mutant of zebrafish hearts was examined in wildtype and double *flcna* $^{exon\ 1-/-}$ + *flcnb* $^{exon\ 14-/-}$ mutant embryos by TEM. The ultrastructure results showed that myofibrils in the wildtype hearts were regularly arranged in repeated sarcomere units, whereas in hearts of double mutant embryos, fewer myofibrils were uniformly aligned in successive sarcomeres. Myofibril bundles were slimmer and branched irregularly. Additionally, many Z-discs were zigzagged in appearance, contained gaps, were fainter or missing. These data demonstrated that in *FLNC* mutant embryos, the initiation of early sarcomerogenesis occurred but did not proceed normally,

leading to fewer stable myofibrils and resulting in the dissolution of others. Collectively, Dr. Alnefaie concluded that *flnc* is required for Z-disc formation and arrangement.

The hypothesis that *flnc* is required for cardiomyocyte morphogenesis is supported by the cardiac phenotypes observed in the double mutants. In the double mutants, cells located in the center of the ventricular chamber showed an increase in the cell cross-sectional area and were elongated compared to wildtype. This finding confirmed the role of *flnc* in ventricle cardiomyocyte size and shape(Alnefaie 2019). In addition, based on the location of Flnc actin-binding protein, Dr. Alnefaie investigated the arrangement of actin filaments. The FLNC protein links cortical actin to integral membrane proteins, which are in turn linked to ECM. These connections help secure the components of the Z-disc to the actin cytoskeleton (Stossel, Condeelis et al. 2001). By fluorescently labeling actin, Dr. Alnefaie observed that wildtype cardiomyocytes assembled sarcomeric actin in parallel, tightly packed, stiff, thick bundles. These appeared as periodic units consistent with successively arranged sarcomeres. In contrast, sarcomeric actin bundles in the double *FLNC* mutant embryos were overall more difficult to discern, thinner, less dense, and in some cases, curved. In both ventricle and atrium, the global organization of actin fibers was disrupted. In summary, Dr. Alnefaie's study demonstrates that *FLNC* plays an essential role in sarcomerogenesis in cardiomyocytes, particularly in Z-disc formation and the actin cytoskeleton arrangement. These are the first data to demonstrate the sarocmerogenesis role in the heart, and the first in vivo data (as opposed to cultured cells), to be reported.

In this study, I used zebrafish mutant lines to investigate how FLNC directly or indirectly affects development of the atrioventricular (AV) valve. Prior studies showed that a decrease in retrograde or oscillatory flow through the developing atrioventricular valve decreased the expression of flow-responsive genes in AV endocardial cells, and interfered with valve

specification at 48 hpf.(Vermot, Forouhar et al. 2009) Of note, morpholino knockdown of *flncb* led to increased reverse flow fraction (RFF) at the AVJ (Begay, Tharp et al. 2016), but little data indicate whether or not increased RFF is pathologic. This project will test the overarching hypothesis that *flnc* depletion causes changes in RFF, which lead to aberrant valve development, which in turn affects overall heart function.

In Aim 1: Examine the effect of *flnc*-depletion on the contractile properties of the heart and determine how RFF is altered.

Rationale: In previous studies, *flncb* MO knockdown embryos at 48 hpf exhibited a significantly increased heart rate, but no significant change in stroke volume or cardiac output(Begay, Tharp et al. 2016). These embryos also exhibited a ~3-fold increase in RFF over controls, a significant difference. The impact of *flnca* knockdown, or double gene knockdown, upon RFF has not been investigated. We hypothesize that the loss of *flnc* will weaken costamere function in cardiac chambers, which in turn will affect pumping efficiency in the heart, alter contractile patterns in *FLNC* mutants, and thereby increase RFF. If true, these changes may trigger compensatory responses in the heart, such as hypertrophy, that provide insight into patient's development of cardiomyopathy later in life.

Approach:

A high-speed video camera captured contraction in live hearts of mutant or wildtype embryo hearts (53 hpf). Cardiac motion and blood movement were analyzed by Matlab to determine functional parameters such as RFF, stroke volume, heart rate and cardiac output.

Aim 2: Examine the effect of *flnc* depletion on the transcriptional response of flow-responsive genes, and investigate AV valve differentiation.

2.1 Does altered flow effect expression of klf2a and *klf2b?*

Rationale: Prior work showed that loss of RFF via *gata1* knockdown decreased expression of the transcription factor *klf2a*, and that loss of flow (forward or reverse) decreased expression of transcription factor *egr1*(Vermot, Forouhar et al. 2009, Banjo, Grajcarek et al. 2013). Prior work by Molly Zeller from our group indicated that that loss of RFF via *gata1* knockdown had no effect on expression of the paralogous gene, *klf2b*. Whether *egr1* and *klf2b* detect and respond to increased RFF, as does *klf2a*, is not known.

Hypothesis: We hypothesize that mutations in *flnc* lines will increase expression of *klf2a*, but not *klf2b* and *egr1*.

Approach:

We will use qPCR to measure the expression level of these genes in *flnc* mutants at 53 hpf, a time near the end of the developmental window when RFF is present.

2.2 How is valve differentiation affected by disruption of FLNC?

Rationale: Dr. Alnefaie's data indicated that embryos homozygous for *flcna* $^{exon1-/-}$ mutation exhibited no overt cardiac phenotypes. Embryos homozygous for *flcnb* $^{exon14-/-}$ exhibited a significantly slower heart rate and impairment of sarcomere Z-discs. Embryos homozygous for *flcnb* $^{exon\ 35-/-}$ exhibited more frequent and more severe overt cardiac phenotypes (edema and visual heart morphology). Valve differentiation has not been analyzed in any *flnc* animal model to date. We predict that a correlation exists between the degree of RFF, the strength of the cardiac phenotype and the presence of valve differentiation defects.

Hypothesis: We hypothesize that embryos homozygous for *flcnb* $^{exon14-/-}$ or *flcnb* $^{exon\ 35-/-}$ may exhibit impairment of valve differentiation, and that impairment will be worse in *flcnb* $^{exon\ 35-/-}$, which have the more severe phenotype.

Approach:

Immunocytochemistry (ICC) with ALCAM antibody at 53 hpf; *Tg(fli1:eGFP)* transgenic fish. ALCAM antibody (red) labels all myocardial cells, as well as any differentiating endocardial . GFP (green) labels the endocardium layer. Thus, during the valve development, we can identify green+red differentiating endocardial cells, and observe any changes in cell shape and number.

Aim 3. Determine whether *flnc* mutation leads to protein aggregation in cardiomyocytes.

Rationale: In MFM disease affecting skeletal muscle, the production of protein aggregates is a hallmark of the disease. Some studies indicate that aggregates arise in cardiomyocytes as well (Valdés-Mas, Gutiérrez-Fernández et al. 2014), but this varies with the allele. In humans, a recent study proposes that all Flnc truncation mutants undergo nonsense-mediated decay. If they are not translated, they would represent null mutants, thus supporting protein insufficiency as the underlying mechanism contributing to DCM. However, it has not been verified in animal systems whether truncation mutants are uniformly not translated. If translated, the truncated might proteins misfold, and facilitate aggregate formation which negatively impacts cell function. Little data indicate whether the truncated proteins have partial function that may rescue or ameliorate some *flnc* phenotypes. Ruparelia and colleagues found that homozygous *flncb* (*sot*) mutants (a truncation mutant) produced myosin-positive and desmin-positive protein aggregates in skeletal muscle (Ruparelia, Zhao et al. 2012). The authors did not directly confirm the

translation of *sot* protein and its presence in the aggregates. Moreover, the heart tissue was not investigated by these authors.

Hypothesis:

We hypothesize that homozygous *flcnb* $^{exon\ 14-/-}$ and *flcnb* $^{exon\ 35-/-}$ mutants produce a truncated protein product, which forms myosin-positive and desmin-positive intracellular aggregates in cardiomyocytes, and that these aggregates may exert a toxic effect that explains why the above alleles are more severe in phenotype than *flcnb* $^{exon1-/-}$.

Approach:

Immunocytochemistry (ICC) experiments to label candidate proteins (myosin and desmin) that may aggregate in *flnc*-depleted cells. ICC experiments will test the presence of desmin (costamere component) and myosin (sarcomere component) in aggregates. We examined homozygous *flnc*b $^{exon\ 14-/-}$ mutants, homozygous *flcnb* $^{exon\ 35-/-}$ mutants, or double homozygous *flcna*$^{exon\ 1-/-}$ *flcnb* $^{exon\ 14-/-}$ mutants.

CHAPTER 2: INTRODUCTION

Cardiovascular diseases (CVDs) are characterized as heterogenous cardiac diseases, and represent a major human health concern (Go, Mozaffarian et al. 2013). Dilated Cardiomyopathy (DCM) is the most common type of cardiomyopathic disease. The prevalence is estimated to be 4.5 cases per 100,000 per year**.** DCM is characterized by a dilated left ventricular chamber and systolic dysfunction that results in congestive heart failure (Watkins, Ashrafian et al. 2011, Merlo, Cannata et al. 2018). In the last few years, FLNC has been linked to several cardiomyopathic diseases (Ortiz-Genga, Cuenca et al. 2016). However, the functional relationship between cardiomyopathy and FLNC is not fully understood (Begay, Tharp et al. 2016, Brodehl, Ferrier et al. 2016).

FLNC is a dimeric actin crosslinking protein that plays a critical role in actin organization and stabilization of th emembrane associated cytoskeleton. FLNC acts as a scaffold for many cytoskeletal structural and signaling proteins (Brodehl, Ferrier et al. 2016). It is expressed exclusively in the cardiac and skeletal muscle. Moreover, high amounts of FLNC protein is found in the in Z-discs, cardiac intercalated discs and skeletal muscke myotendinous junctions while low amounts of FLNC attach the cortical actin cytoskeleton to plasma membrane proteins (Gomer and Lazarides 1981, van der Ven, Obermann et al. 2000).

One study used mice as a model to investigate the role of FLNC in myofibril development. The limitation of this study is that the mice died right after birth due to respiratory failure, and potential cardiac defects, if any, were not reported (Dalkilic, Schienda et al. 2006). Medaka has also been used as a model organism examine the role of FLNC in the heart and skeletal muscle development; this study demonstrated cardiac phenotypes in homozygous *flnca* mutants (Fujita, Mitsuhashi et al. 2012). Zebrafish has proven a robust model organism to help elucidate genetic

and molecular aspects of human disease. Especially, it is suited for developmental cardiovascular studies due to several features that enable researchers to study early developmental defects which can be difficult to examine in other vertebrate models including mouse (Ruparelia, Zhao et al. 2012). The zebrafish *sot/flncb* mutant exhibits broken muscle fibers and the skeletal muscle exhibits protein aggregation. Although the *sot* allele encodes a potential truncated protein, the phenotypes observed by Ruparelia and colleagues were not demonstrated to be full loss of function versus partial loss of function phenotypes, and this study did not examine the heart. To better understand the effects of losing *flnc* function in cardiac muscle, mutant lines for *flnc* were investigated for the two zebrafish paralogous *flnc* genes (*flnca* and *flncb*)(Alnefaie 2019).

The present study makes use of 4 novel nonsense alleles in zebrafish *flnca* and *flncb.* Theses alleles are: $flnca^{exon1}$ and $flncb^{exon1}$, which each encode a nonsense mutation within the N-terminal actin binding domain. The $flncb^{exon14}$ and $flncb^{exon35}$ alleles encode nonsense mutation within the 4rth and 17th immunoglobulin-like domains, respectively. The previous dissertation work performed by Dr. Rasha Alnefaie determined that the two presumed null alleles, $flnca^{exon1}$ and $flncb^{exon1}$, did not exhibit cardiac phenotypes whereas the alleles presumed to encode truncated proteins, $flncb^{exon14}$ and $flncb^{exon35}$, appeared to have stronger phenotypes in both heart and skeletal muscle.

Here, we evaluated whether homozygous loss of a single flnc paralog affects contractile properties of the heart, and what impact this has on valve function. Previously, Begay and colleagues found that knockdown of *flncb* by antisense morpholino resulted in significantly increased reverse flow (RF) (Begay, Tharp et al. 2016). The first goal of my project was to use the available mutant lines to comparatively analyze functional heart properties including heart rate, stroke value, cardiac output an reverse flow fraction.

In addition, potential alterations in reverse flow may impact heart valve development or function in a *flnc* mutant backgrounds . A study by Vermot and colleagues revealed that too little reverse flow led to abnormal valve development (Vermot, Forouhar et al. 2009). In our study with Begay, the morpholino data suggested that the opposite effect (too much RF) was present. To assess AV development, the number of specified endocardial valve cells, the cell area, and the degree of cell circularity were examined in *flnc* mutants, compared to controls. Finally, in wildtype or double mutant *flnca*^{exon1}; *flncb*^{exon14} hearts, we analyzed a flow-responsive transcription factor, *klf2a,* and it paralog, *klf2b,* via qPCR to identify whether changes in expression levels occur in response to increased reverse flow. (Dekker, van Thienen et al. 2005). Altogether, our study will determine whether and how FLNC function increases retrograde flow, and whether and how it impacts heart valve function.

Previous studies in mice, Medaka and zebafish showed that insoluable cytoplasmic aggregates form in the skeletal muscle of *flnc* mutants. In humans, several FLNC mutant alleles lead to potentially toxic protein aggregates, and patients with these alleles showed cardiac and/or skeletal muscle phenotypes(Vorgerd, van der Ven et al. 2005). Additionally, Several studies have shown that patients with MFM develop protein aggregates related to FLNC in cardiac muscle (Valdés-Mas, Gutiérrez-Fernández et al. 2014, Brodehl, Ferrier et al. 2016). Protein aggregates may be described as the accumulation of misfolded mutant proteins, as well as other large proteins, in the cytoplasm. Extensive formation of protein aggregates may be toxic and may lead to muscle degeneration (Aguzzi and O'Connor 2010). Mutations in the protein interaction sites or dimerization domains of FLNC can lead to the accumulation of several muscle proteins in insoluble cytoplasmic aggregates such as desmin and actin(Dalkilic, Schienda et al. 2006, Ruparelia, Zhao et al. 2012). A prior histological sectioning study from our group, did not show

evidence of protein aggregation in *flncb*^{exon35} mutant zebrafish at 48 hpf. However, this study was limited in that the 48 hpf heart has developed only a single layer of myocardium, and the hearts themselves are only about 1 mm in diameter. H and E stained sections may not have the resolution requiredn to determine conclusively whether aggregated proteins were present, due to the small size of the cells and the limited amount of cardiac tissue available at this stage(Alnefaie 2019). In an alternative approach, we performed immunocytochemistry (ICC) with antibodies to two candidate proteins, desmin and myosin, to examine the colocalization of these two proteins with intracellular puncta. The goal of this study was to determine whether these Z- disc proteins identify and contribute to aggregates or not.

CHAPTER 3: RESULTS

Measurement of the biomechanical phenotypes associated with three novel nonsense *flnc* alleles in mutant zebrafish hearts.

Flnc is actin binding protein that localizes to the sarcomere. In this location, it may play a role in contractility and the ability of sarcomeres to withstand mechanical stress during cardiac contraction. We captured videos in live embryonic hearts at 53 hpf for different *flnc* genotypes, including: *flnca*$^{exon1-/-}$,*flncb*$^{exon14-/-}$, *flncb*$^{exon35-/-}$and wildtype embryos. We assessed four functional measures: heart rate, stroke volume, cardiac output and reverse flow fraction.

In *flncb*$^{exon14-/-}$hearts, the heart rate (133.1 bpm) was higher than wildtype (125.5 bpm) but not significantly different (P = 0.45) (Fig 3.1A). The stroke volume (0.3 nl) was significantly decreased compare to the wildtype embryos (0.5nl), a significant difference (P = 0.002) (Fig 3.1 B). Similarly, cardiac output (31.2 nl/min) was significantly decreased compared to wildtype embryos (69.29. nl/min) (P = <0.001) (Fig 3.1C). The reverse flow fraction in *flncb*$^{exon14-/-}$ hearts (0.01) did not exhibit a significant difference relative to wildtype hearts (0.02) (P =0.87) (Fig 3.1 D and Video1, 2). These data indicate that *flncb*$^{exon14-/-}$embryos exhibited reduced cardiac efficiency but that RF was not affected.

We next evaluated *flncb*$^{exon35-/-}$embryos. The heart rate in mutant embryos (132.7 bpm) compared to wildtype embryos (125.5 bpm) was notnot significantly different (P = 0.47) (Fig 3.2A). *flncb*$^{exon35-/-}$ hearts exhibited no differences in stroke volume (0.5nl) compared to wildtype (0.5nl) (P = 0.80) (Fig 3.2 B). Likewise, the cardiac output (55 nl/min) displayed no differences relative to wildtype (69.29. nl/min) (P = 0.67) (Fig 3.2 C).

The reverse flow fraction in *flncb*$^{exon35-/-}$ mutant hearts (0.02) was variable, but the increase was non-significant relative to wildtype (0.01) (P = 0.66) (Fig 3.2D). These results revealed that *flncb*$^{exon35-/-}$ hearts do not develop functional differences at 53 hpf.

Homozygous *flnca*$^{exon1-/-}$ hearts showed variability in the heart rate (116.2 hpm) relative to wildtype embryos (125.8 bpm) but the means were not significantly different (P = 0.42) (Fig 3.3A). Stroke volume in mutants (0.64nl) was not different relative to wildtype (0.5 nl) (P = 0.78). The cardiac output (67.2 nl/min) was not different relative to wildtype (69.29.nl/min) (P = 0.78). The reverse flow fraction in the *flnca*$^{exon1-/-}$ hearts exhibited a non-significant increase (0.05) compared to wildtype (0.02) (P = 0.19) (Fig 3.3B-D). These results showed that *flnca*$^{exon1-/-}$ hearts do not develop functional differences at 53 hpf.

In sum, these experiments demonstrate that mutant hearts showed more variability than controls in several functional parameters, yet the means did not statistically differ. We speculate that cardiac cells may have been impacted by loss of one *flnc* paralog, but typically were able to compensate such that function remained within normal ranges.

Stress experiment:

We hypothesized that mutants raised under sensitized conditions may exhibit enhanced phenotypes too subtle to detect under optimal conditions. In this case, the presence of intact Flnca protein is likely to compensate for depletion of Flncb protein, but the potentially compromised cardiac integrity may become apparent when the heart is forced to work at increased capacity. At 40 hpf, the homozygous *flncb*$^{exon35-/-}$ mutant embryos were subjected to temperature stress via incubation at 37° C for 13 hrs. High-speed videos were taken ventrally at 53 hpf to compare heart function in stressed *flncb*$^{exon35-/-}$, stressed wildtype and non-stressed

wildtype hearts. The heart rate of stressed wildtype embryos showed no significant increase (126.4 bpm) compared to non-stressed wildtype hearts (127.7 bpm) (P=0.34). The heart rate of stressed *flncb*$^{exon35-/-}$ embryos demonstrated a slight but non-significant increase (136.3 bpm) compared to the heart rate of stressed wildtype hearts (126.4 bpm) (P=0.08) (Fig 3.4A). The stroke volume of non-stressed versus stressed hearts did not differ, Stressed *flncb*$^{exon35-/-}$ hearts demonstrated a significant decrease in stroke volume (0.4 nl) compared to non-stressed wildtype (0.6 nl) (P=0.04),but curiously there was no significant differences between stroke volume (0.4 nl) of stressed *flncb*$^{exon35-/-}$ and stressed wildtype (0.5 nl)(P=0.78) (Fig 3.4 B). Stressed *flncb*$^{exon35-/-}$ hearts exhibited significantly decreased in cardiac output (55.0 nl/min) compared to non-stressed wildtype (73.4.2. nl/min) (P=0.02), but no significant differences when compared to stressed wildtype (65.1 nl/min) (P=0.93) (Fig 3.4 C). Finally, the reverse flow fraction in stressed *flncb*$^{exon35-/-}$ hearts (0.02) did not differ relative to non-stressed wildtype hearts (0.011) (P=0.07) or stressed wildtype hearts (0.029) (P=0.58) (Fig 3.4D). In summary, these experiments demonstrate that stressed wildtype embryos exhibited normal heart function, and therefore the stress condition itself is not limiting. The experiment identifies a potential decreased in SV and CO in stressed *flncb*$^{exon35-/-}$ hearts. However, this conclusion is tentative, since the differences in mutants were apparent only when compared to non-stressed wildtype hearts, not stressed wildtype hearts.

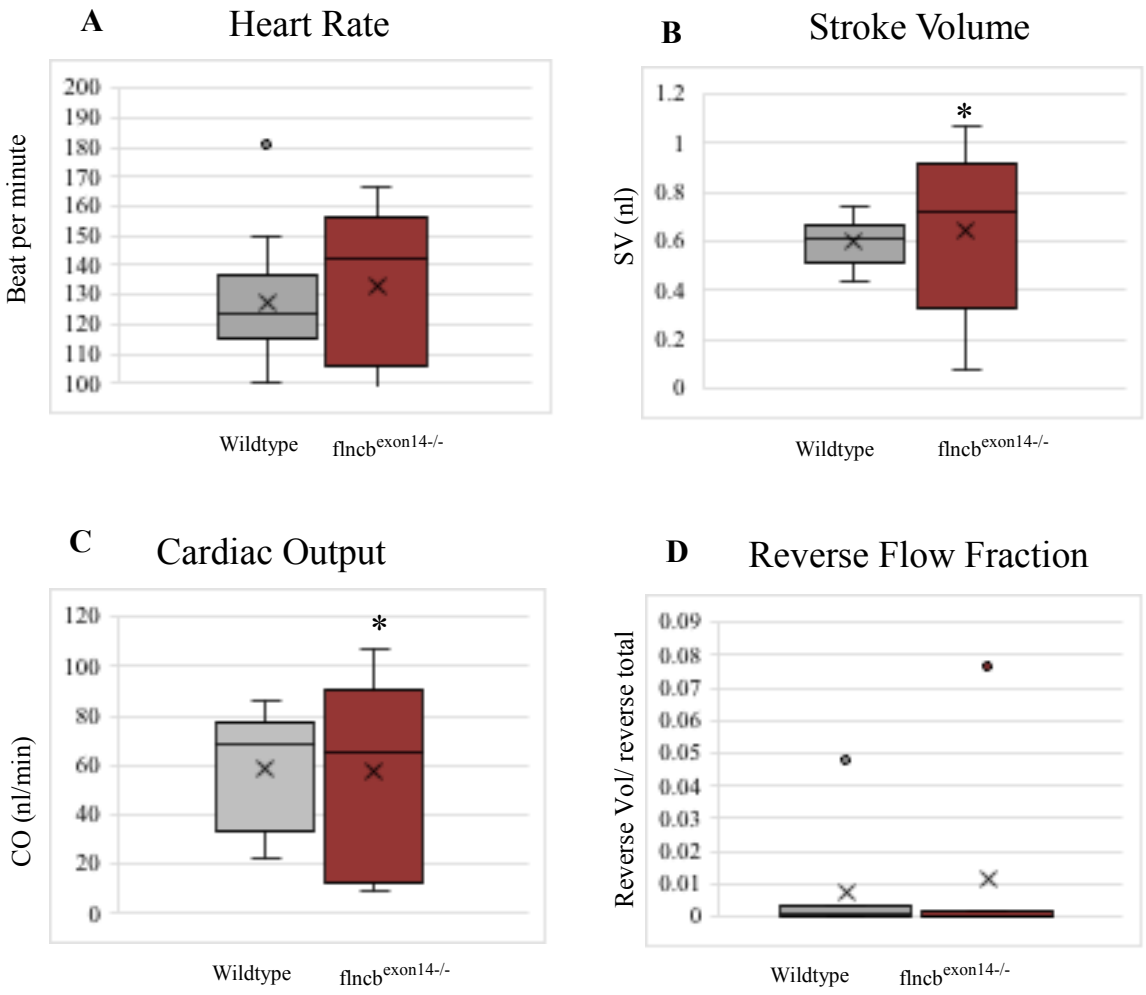

Figure 3.1 *flncb*$^{exon14-/-}$ mutants exhibit cardiac function defects at 53 hpf. High-speed videos and MATLAB software were used to examine CO, HR, RV, and SV in embryonic hearts at 53 hpf. (A) Relative to the wildtype average HR (133.1 bpm), *flncb*$^{exon14-/-}$ hearts exhibited no significant difference in HR (P = 0.45)(125.5bpm). (B) The SV of *flncb*$^{exon14-/-}$ hearts was significantly decreased relative to wildtype hearts (One Way ANOVA P = <0.001). (C) The CO of *flncb*$^{exon14-/-}$ hearts was significantly decreased compared to wildtype hearts (One Way ANOVA, P = 0.002). (D) The RF fraction of *flncb*$^{exon14-/-}$ mutant hearts displayed no differences compared to wildtype hearts (P =87). n=9. HR=heart rate, CO= cardiac output, SV=stroke volume, RF=reverse flow, bpm= beats per minute

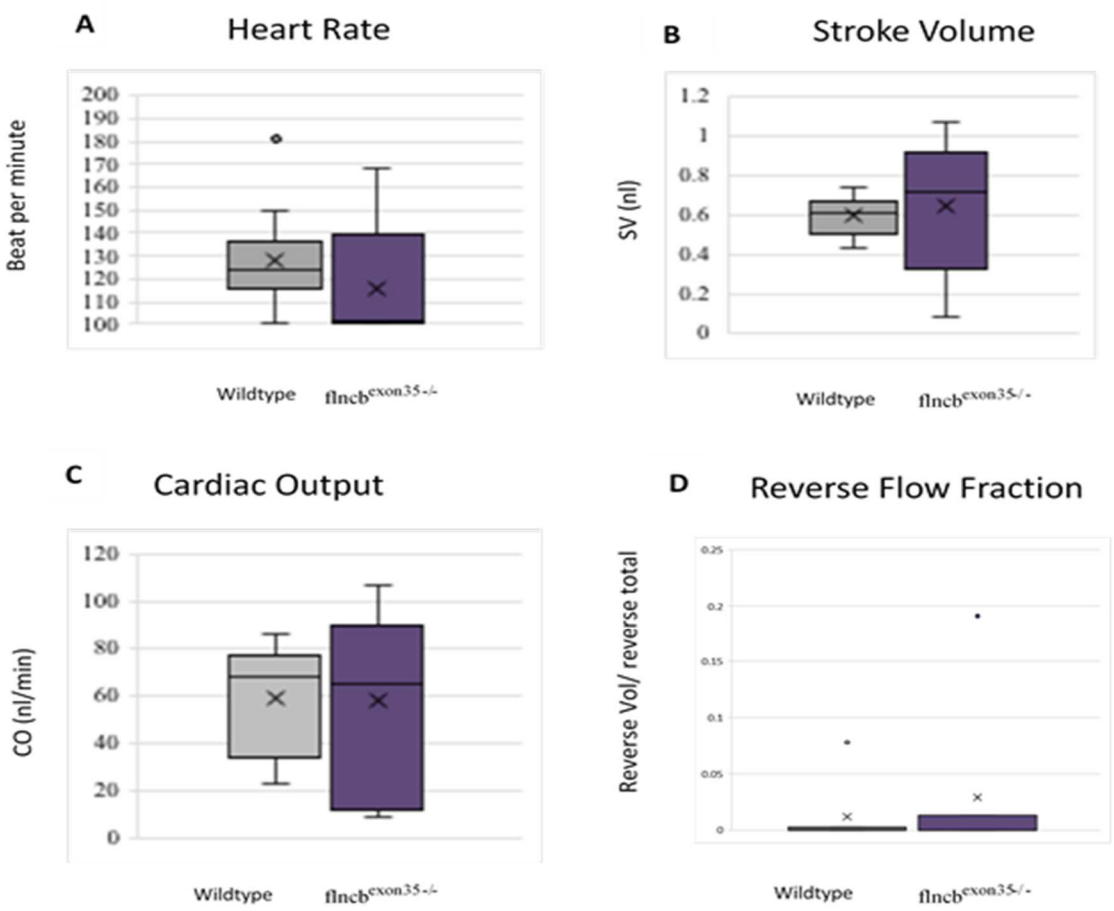

Figure 3.2 *flncb*$^{exon35-/-}$ mutant hearts exhibited no differences in cardiac function at 53 hpf. High-speed videos and MATLAB software were used to examine the effects of phenotypes on heart function (CO, HR, RV, and SV) at 53hpf. (A) Relative to the wildtype average HR (132.7 bpm), *flncb*$^{exon35-/-}$ exhibited no significant change in HR (125.5 bpm) (P = 0.47). (B) SV of *flncb*$^{exon35-/-}$ embryos was normal relative to wildtype (P = 0.80). (C) CO of *flncb*$^{exon35-/-}$ embryos was normal relative to wildtype (P = 0.67). (D) The RF fraction of *flncb*$^{exon35-/-}$ mutant hearts showed variability but no significant increase in the mean relative to wildtype hearts (P = 0.66). n=8. HR=heart rate, CO= cardiac output, SV=stroke volume, RF=reverse flow, bpm= beats per minute.

.

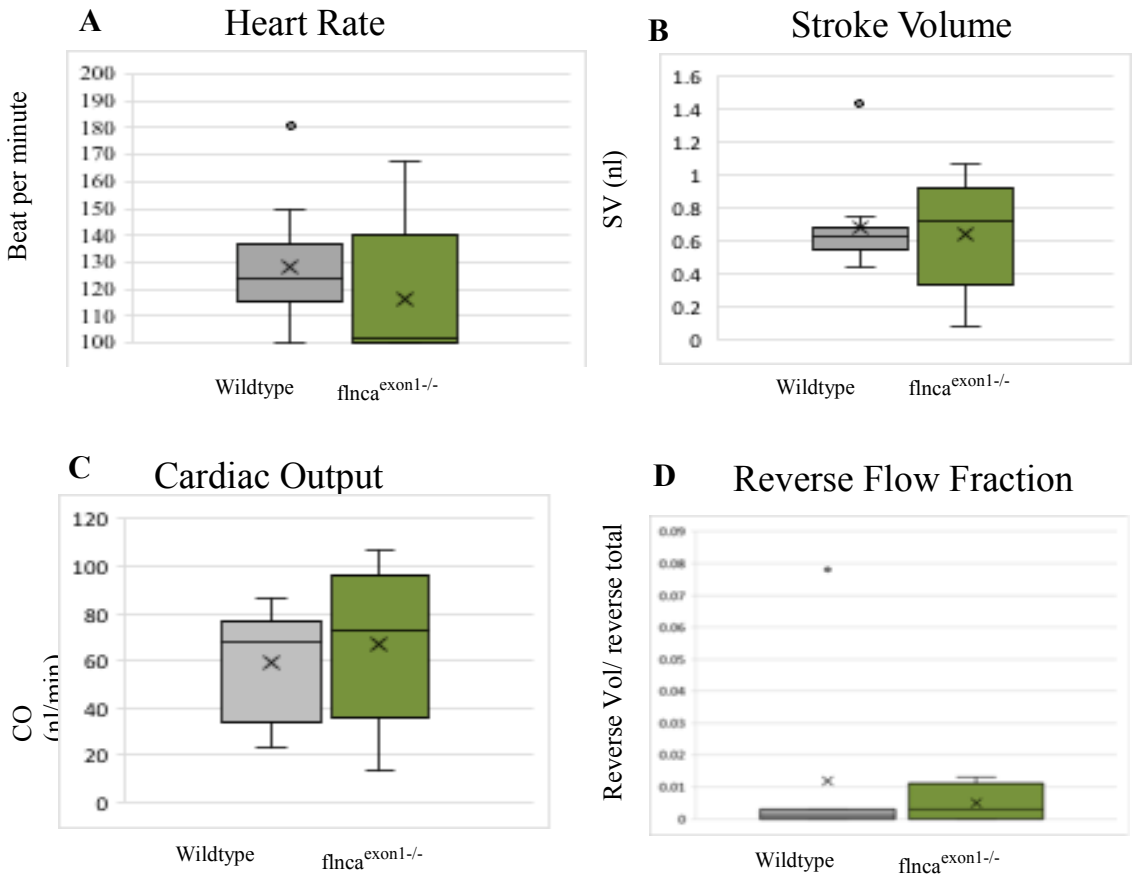

Figure 3.3 *flnca*$^{exon1-/-}$ mutants exhibit no difference in cardiac function at 53 hpf. High-speed videos and MATLAB software were used to examine the effects of phenotypes on heart function (CO, HR, RV, and SV) at 53 hpf. (A) Relative to the wildtype average HR (125.5 bpm), *flnca*$^{exon1-/-}$ exhibited no significant change in HR (112.5bpm) (P = 0.42). (B) The SV of *flnca*$^{exon1-/-}$ embryos was normal relative to wildtype (P = 0.78). (C) The CO of *flnca*$^{exon1-/-}$ embryos was normal relative to wildtype (P = 0.78). (D) The RF fraction of *flnca*$^{exon1-/-}$ mutant hearts showed a slight but non-significant increase relative to wildtype (P = 0.19). n=5. HR=heart rate, CO= cardiac output, SV=stroke volume, RF=reverse flow, bpm= beats per minute.

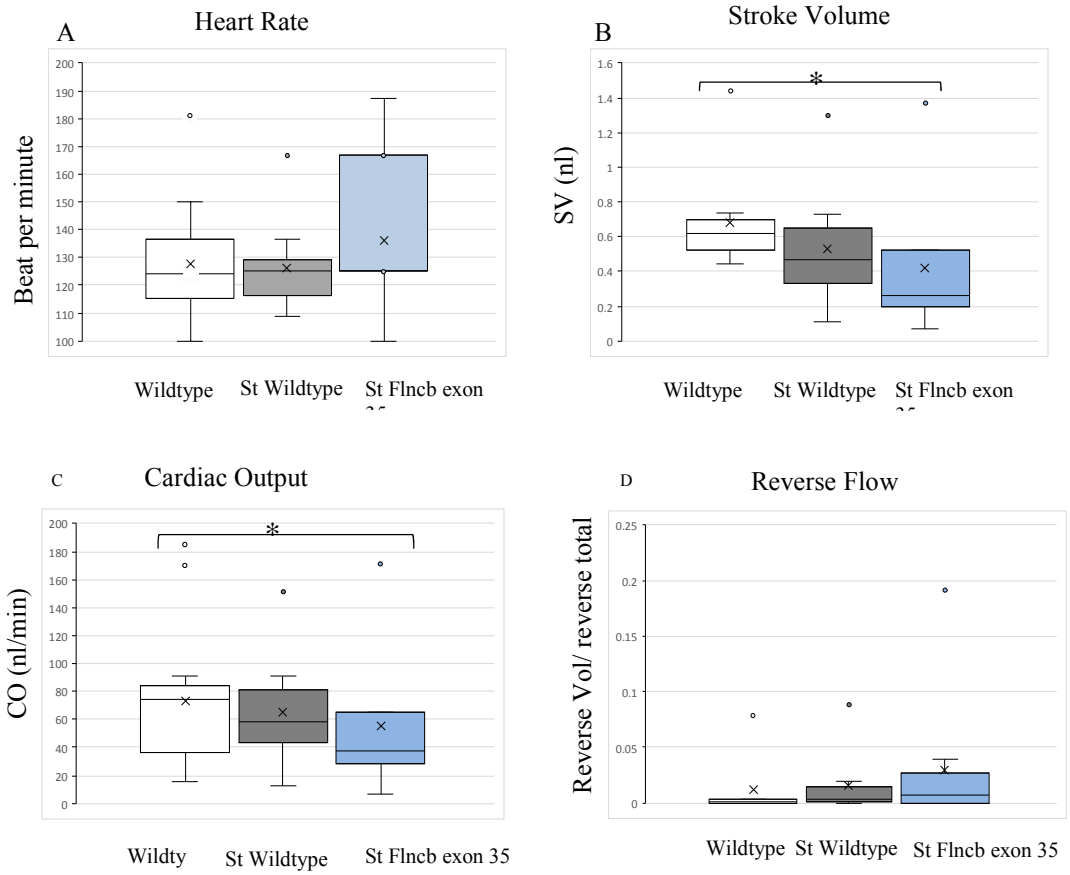

Figure 3.4 Stressed *flncb*$^{exon35-/-}$ mutants exhibited potential differences in cardiac function on the heart at 53hpf. (A) Relative to the average HR in wildtype (127.7 bpm) and stressed wildtype (126.4 bpm) hearts, stressed *flncb*$^{exon35-/-}$ hearts exhibited slight no significant change in HR (136.3 bpm). (B) The SV of stress *flncb*$^{exon35-/-}$ hearts was significantly decreased relative to non-stressed wildtype hearts (average SV 0.41 nl and 0.68 nl, respectively; One Way ANOVA P=0.029). (C) The CO of stressed *flncb*$^{exon35-/-}$ hearts was significantly decreased compared to non-stressed wildtype hearts (average CO 73.4 nl/min and 0.55 nl/min, respectively; One Way ANOVA P=0.047.) (D) The RF fraction of stressed *flncb*$^{exon35-/-}$ mutant hearts showed no change relative to wildtype hearts and stressed wildtype hearts (average RF 0.011, 0.015 and 0.029, respectively). n=8. HR=heart rate, CO= cardiac output, SV=stroke volume, RF=reverse flow, bpm= beats per minute.

Mechanotransduction: The genetic response to altered flow in FLNC mutants:

During valve development, biomechanical cues are generated within the embryonic heart by blood flow that are required for the development of the atrioventricular valve (Aikawa, Whittaker et al. 2006, Haack and Abdelilah-Seyfried 2016). Endocardial cells directly interact with flowing blood and may be sensitive to the disruption of hemodynamic patterns. In particular, cells in the developing of AV constriction are subjected to relatively high levels of shear stress. Previous work has shown that the degree of retrograde flow (RF) through the developing AV valve affects its development. In embryos injected with *flncb* morpholino, Begay and colleagues showed significantly increased reverse flow (Begay, Tharp et al. 2016). In other experiments, valve abnormalities could be observed in 96 hpf hearts that exhibited reduced reverse flow at 48 hpf (Vermot, Forouhar et al. 2009). To examine the biomechanical response to the perturbed flow in *flnc* mutants, we performed two experiments: 1) a dual labeling immunohistochemistry procedure to assess the specification of endocardial valve cells. These experiments used the transgenic line *Tg(fli1:eGFP)* in which the *fli1* promoter drives the specific expression of eGFP in endothelial cells of blood vessels and heart. GFP-positive endocardial cells that concommitantly express ALCAM are classified as differentiating valve cells, 2) qPCR was used to examine the alteration in expression of the flow-responsive gene *klf2a* and its paralog *klf2b*.

Immunohistochemistry with ALCAM in an endocardial specific transgenic line.

The number of ALCAM-expressing endocardial valve cells in 53 hpf embryo were counted at the superior and inferior valve leaflets. In addition, ImageJ software was used to calculate the cross-sectional area and the shape of AV endocardial cells in dissected hearts at 53 hpf for

several genotypes: *Tg(fli1:eGFP)* control, *flncb*$^{exon14-/-}$ *Tg(fli1:eGFP)* mutants and *flncb*$^{exon35-/-}$ *Tg(fli1:eGFP)* mutants (Fig 3.5A-C). A circularity value of 1.0 represents a perfectly round cell, whereas smaller values indicate elongated polygon shapes. The average number of ALCAM-expressing endocardial cells in the *flncb*$^{exon14-/-}$ *Tg(fli1:eGFP)* was significantly decreased compared to *Tg(fli1:eGFP)* control hearts (8 versus 15 cells, respectively) ($P < 0.001$). *flncb*$^{exon35-/-}$ *Tg(fli1:eGFP)* hearts likewise showed a significant decrease in the number of ALCAM-expressing endocardial valve cells relative to *Tg(fli1:eGFP*) control hearts (11 versus 15 cells, respectively; $P = 0.002$)(Fig 3.5D). Comparing the number of ALCAM-expressing endocardial valve cells in *flncb*$^{exon14-/-}$ *Tg(fli1:eGFP)* versus *flncb*$^{exon35-/-}$ *Tg(fli1:eGFP)* hearts to each other showed no significant differences. Moreover, the average cell cross-sectional area found in the inferior cushion and the superior cushion did not significantly differ between *Tg(fli1:eGFP*) control and *flncb*$^{exon14-/-}$ *Tg(fli1:eGFP)* hearts (27.81 um^2 versus 32.47 μm^2, respectively, for inferior surface areas, $P = 0.29$; 24,76 μm^2 versus 29.75 μm^2 respectively for the superior cell surface area, $P = 0.115$). In contrast, the average inferior and superior cell cross-sectional area in *flncb*$^{exon35-/-}$ *Tg(fli1:eGFP)* hearts exhibited significant reduction compared to *Tg(fli1:eGFP*) controls (21.03 μm^2 versus 32.47 μm^2 respectively, for inferior surface areas, $P < 0.001$; 21. 75 μm^2 and 29.75 μm^2 respectively, for the superior surface area, $P < 0.001$ (Fig 3.5E).

The circularity of cells in inferior and superior valve regions of *flncb*$^{exon14-/-}$ *Tg(fli1:eGFP)* did not show significant changes compared to *Tg(fli1:eGFP*) controls ($P = 0.28$ and 0.086 respectively). However, the circularity of the inferior region in *flncb*$^{exon35-/-}$ *Tg(fli1:eGFP)* was significantly reduced compared to *Tg(fli1:eGFP*) control ($P = 0.017$)(Fig 3.5F). In sum, these data indicate that valve differentiation defects are apparent in both *flncb*$^{exon14-/-}$ and *flncb*$^{exon35-/-}$

hearts, though more severe in *flncb*$^{exon35-/-}$ hearts. Such changes would be expected to lead to abnormal valve development.

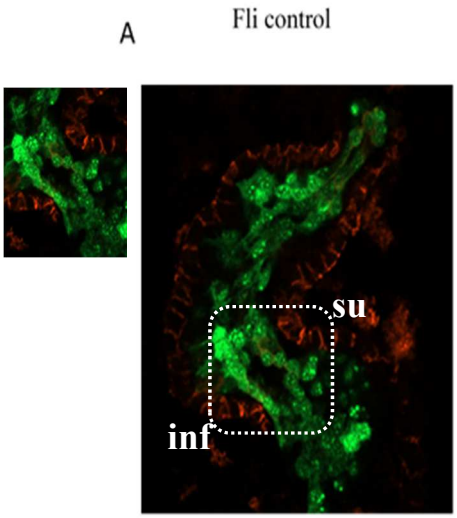

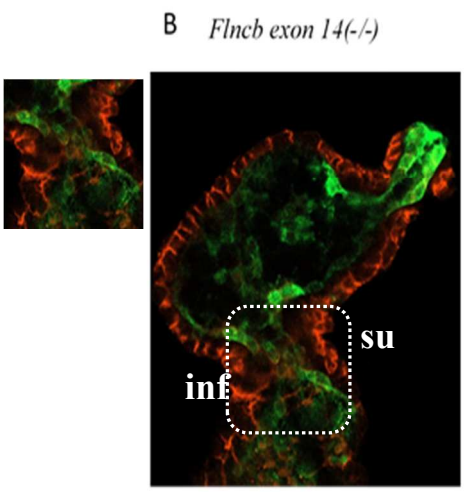

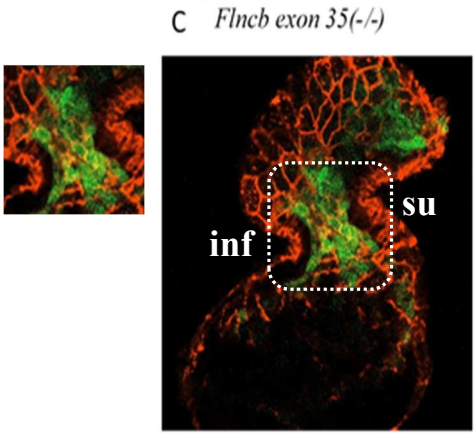

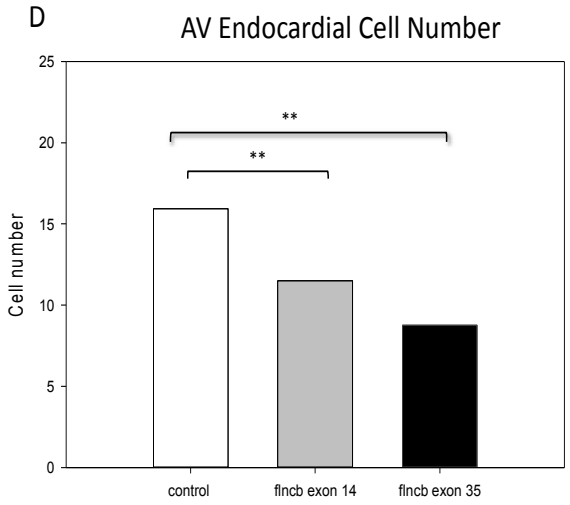

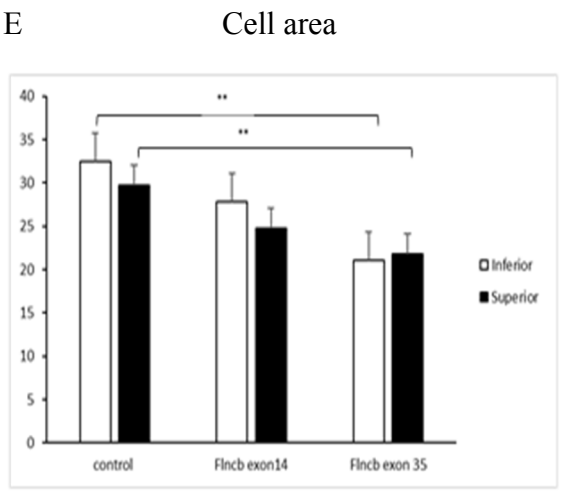

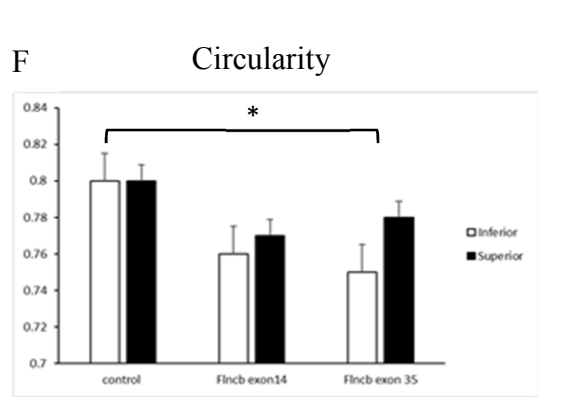

Figure 3.5 Immunohistochemistry with ALCAM in endocardial GFP transgenic line at 53 hpf. (A-C) 3D Images of dissected hearts from *Tg(fli1:eGFP)* control, *flncb*$^{exon14-/-}$ *Tg(fli1:eGFP)* and *flncb*$^{exon35-/-}$ mutant embryos at 53 hpf with ALCAM immunostaining, which labels the myocardial layer in red. Inferior and Superior cushions were identified as defined in Beis et al (2005). (D) Quantification of the number of endocardial valve cells. The *flncb*$^{exon14-/-}$ and *flncb*$^{exon35-/-}$ mutant hearts exhibited significant changes relative to *Tg(fli1:eGFP)* controls (One Way ANOVA, $P < 0.05$, n=8). (E) Quantification of the endocardial valve cell cross-sectional area in both regions (inferior and superior) for individual cells. The *flncb*$^{exon14-/-}$ mutant hearts did not exhibit any significant change relative to *Tg(fli1:eGFP)* control (One Way ANOVA, $P = 0.29$, $P=0.115$, n=8). The *flncb*$^{exon35-/-}$ mutant hearts exhibited significantly decreased cross-sectional area relative to *Tg(fli1:eGFP)* controls (One Way ANOVA, $P < 0.05$, n=8). (F) Quantification of endocardial valve cell shape in both regions (inferior and superior). Higher numbers represent a more circular shape. The *flncb*$^{exon14-/-}$ mutant hearts displayed no significant change compared to controls (One-way ANOVA, $P=0.28$, $P=0.086$ n=8). The *flncb*$^{exon35-/-}$ mutant hearts displayed significant elongated endocardial valve in the inferior region (One Way ANOVA *P <0,05 n=8. Inf = Inferior valve leaflet, Sup = Superior valve leaflet).

Comparative analysis of *klf2a* and *klf2b* expression in *flnc* double mutant hearts

Since our prevous study on fish the doubly injected with *flnca* and *flncb* morpholinos showed a statistically increased reverse flow, we anticipated that RFF would be altered in mutants, and the flow-responsive gene *klf2a*.anticipated might exhibit altered expression (Vermot, Forouhar et al. 2009). To measure the expression level of *klf2a* and *klf2b* in the double *flnca*$^{exon1-/-}$ and *flncb*$^{exon14-/-}$ mutant, we performed Q-PCR using RNA extracted from 53 hpf hearts (Fig 3.6A, B). Assays confirmed that of *klf2a* and *klf2b* are both expressed in cardiac muscle. We found no differences in expression levels of the *ef1a* control gene in hearts of wildtype versus *flnc* double mutant embryos, indicating persistent high levels of mRNA quantity and integrity in all reactions. In the *flnc* double mutant hearts, the expression of both *klf2a* and *klf2b* mRNA was significantly decreased ($P = 0.006$, and 0.009, respectively) (Fig 3.6C, D)

(A)

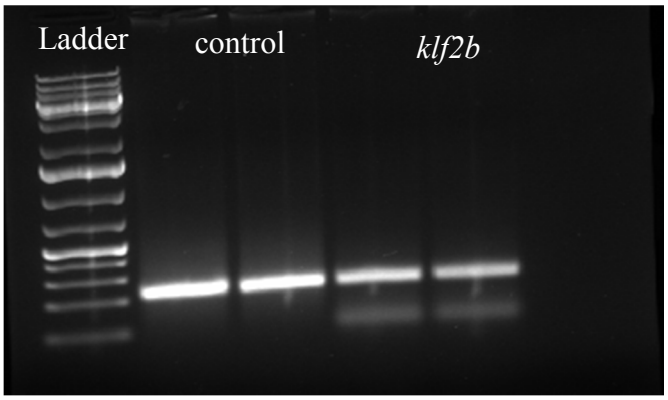

(B

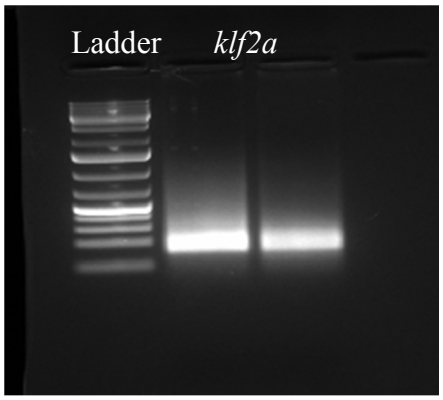

(C)

Fold change of *klf2a*

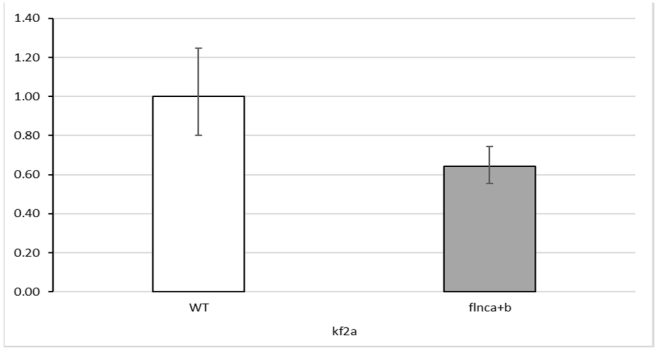

(D)

Fold change of *klf2b*

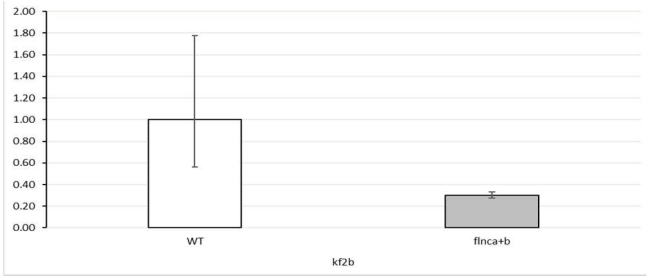

Figure 3.6 Expression level of *klf2a* and *klf2b* in *flnc* double mutants. (A, B) Q-PCR of dissected hearts at 53 hpf. *Elongation factor 1α (ef1α)* was used as a positive control. **(C, D)** Comparison of *klf2a* and *klf2b* expression patterns in double *flnc* mutant hearts.

Assays for protein aggregation in each genotype.

The *flncb*^{exon35} allele creates a nonsense mutation in exon 35 out of 49 total exons, and hence would encode a truncated protein if translated. To determine whether aggregates form in this mutant, we preformed immunohistochemistry using anti-myosin and anti-desmin antibodies on four groups: wildtype, *flncb*$^{exon14-/-}$, *flncb*$^{exon35-/-}$, double mutant, stressed (ST) wildtype and stressed (ST) *flncb*$^{exon35-/-}$. We analyzed the production of protein aggregates in two different ways: counting protein aggregates that are positives for both candadites proteins (desmin and myosin) and counting protein aggregates that are positive for desmin only.

First, we evalulated the number of puncta in the ventricle that were immunopositive for both desmin and myosin (Fig. 3.7G). In the wildtype hearts, we observed rare small puncta which may represent a residual low level of protein aggregation in both desmin and myosin, or a residual degree of background signal (the average number of protein aggregates was 2.12 per ventricle)(Fig 3.7A,J). Wildtype hearts also displayed immunopositive signal near the outflow tract, which may represent background (Fig. 3.7A); therefore, the AVJ region was not included in the counts of aggregates. The number of aggregates in stressed (ST) wildtype hearts was not significantly different relative to wildtype (2.7 versus 2.12 puncta, respectively, P = 0.57). The *flncb*$^{exon14-/-}$ cardiomyocytes displayed no change in the number of protein aggregates compared to wildtype (1.8 versus 2.12 puncta, respectively, P = 0.43), or stressed wildtype (1.8 versus 2.7 puncta, respectively, P = 0.32). The *flncb*$^{exon35-/-}$ cardiomyocytes exhibited no significant increase in protein aggregates relative to wildtype controls (5.3 versus 2.12 puncta, respectively, P = 0.18), and relative to ST wildtype (5.3 versus 2.7 puncta, respectively, P = 0. 208). However, the *flncb*$^{exon35-/-}$ displayed a significant increase relative to *flncb*$^{exon14-/-}$ (5.3 versus 1.8

puncta, respectively, P = 0.03). Of note, ST *flncb*$^{exon35-/-}$ hearts showed a significantly higher average number of protein aggregates relative to wildtype and *flncb*$^{exon14-/-}$ (5, 2.12, 1.8) P = <0.0001). In addition the ST *flncb*$^{exon35-/-}$ showed a significant change relative to ST wildtype (3.5 and 2.8 respectively; P = 0.04). Finally, the number of protein aggregates detected in double *flnc* mutant hearts showed no significant increase relative to wildtype hearts (3.5 and 2.8 respectively; P = 0.94), or ST wildtype hearts (3.5 and 2.12 respectively; P = 0.19).

Next, we evalulated the number of puncta in the ventricle that were immunopositive for desmin but not myosin (Fig. 3.7H). The wildtype as well as St wildtype hearts exhibited a low level of protein aggregation with no significant differences noted (2.6 versus 3; P = 0.53). Similarly, *flncb*$^{exon14-/-}$ cardiomyocytes showed no significant increased in protein aggregation compare to wildtype or ST wildtype (3.4 , 2.2 and 3 respectively; P = 0.24, P = 0.20). The *flncb*$^{exon35-/-}$ cardiomyocytes displayed no difference relative to wildtype (6.14 and 2.6 respectively; P = 0.06). but showed an increased number of protein aggregates relative to ST wildtype (6.14 and 3 respectively; P = 0.03). Notably, ST *flncb*$^{exon35-/-}$ hearts showed increased protein aggregation relative to wildtype, ST wildtype and *flncb*$^{exon14-/-}$ (8.8 versus 2.6, 3, and 3.4, respectively; P = <0,05). Finaly, the double *flnc* mutant hearts displayed no significant change in protein aggregation relative to wildtype (5.4 and 2.6 respectively; P = 0.08), but were increased relative to ST wildtype hearts (5.4 versus 3 ; P = 0.04).

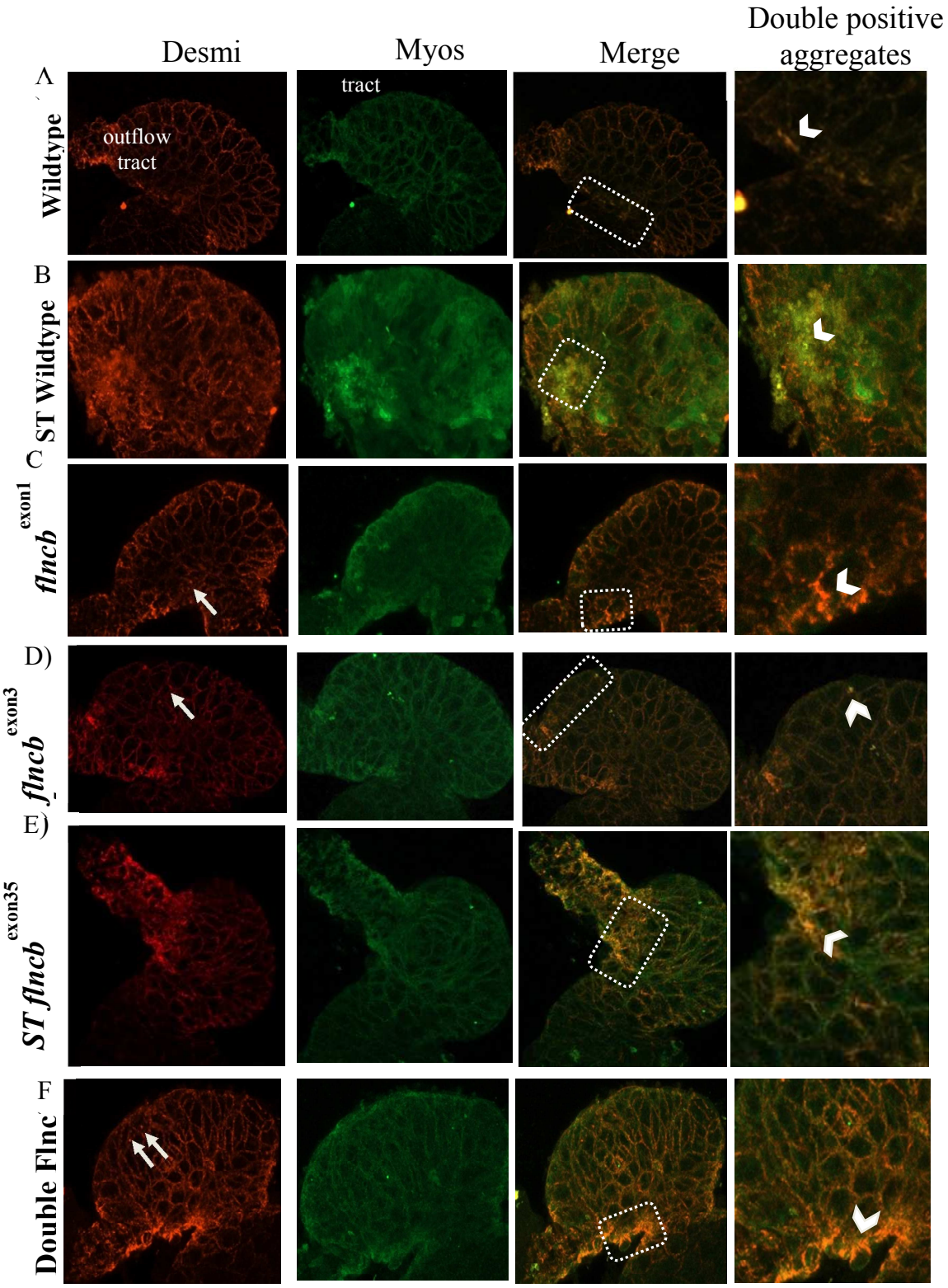
Desmi
Myos
Merge
Double positive aggregates
A
Wildtype
outflow tract
tract
B
ST Wildtype
C
exon1 flncb
D)
exon3 flncb
E)
exon35 ST flncb
F
Double Flnc

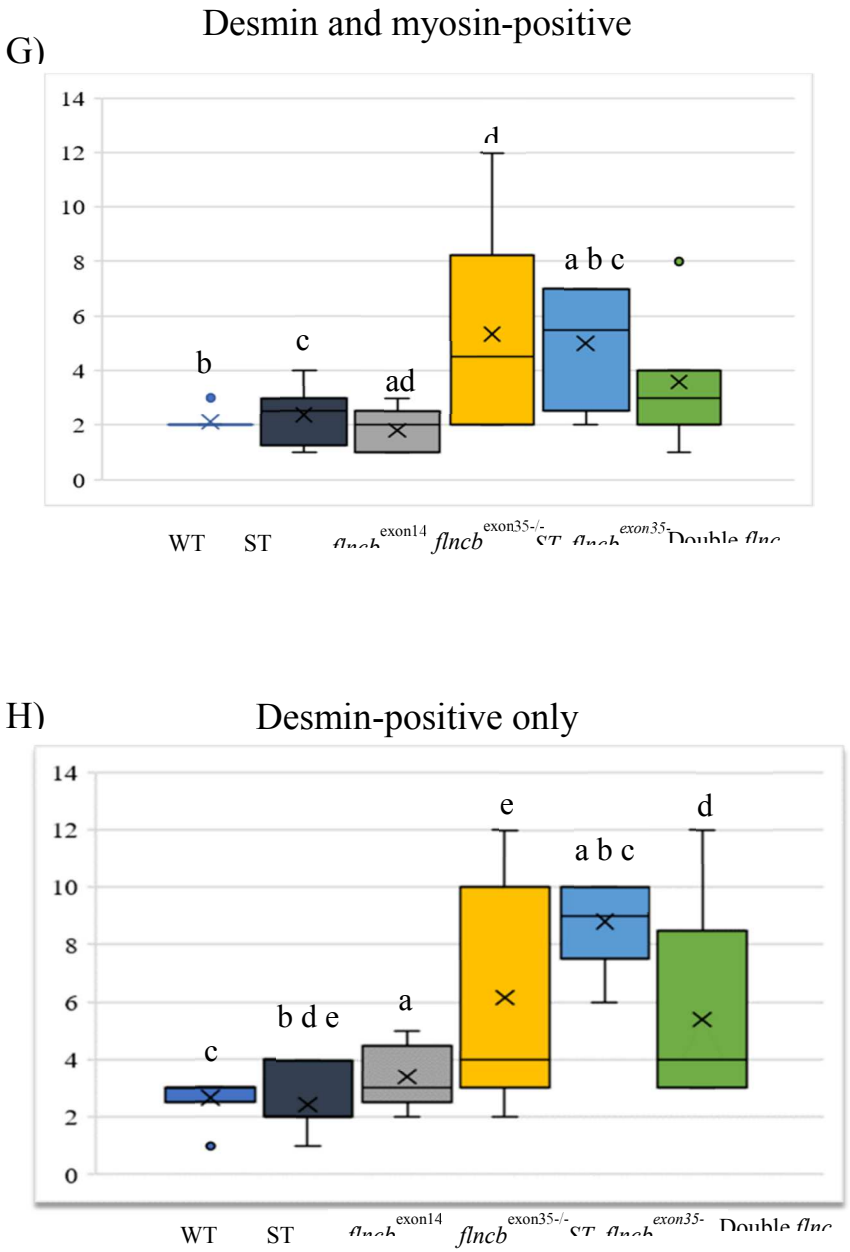

Figure 3.7 Aggregates present in *flnc* mutants heart at 53 hpf. (A-F) Confocal images of dissected hearts from wildtype, St wildtype, *flncb*$^{exon14-/-}$,*flncb*$^{exon35-/-}$, St *flncb*$^{exon35-/-}$ and double *flnc* mutant embryos at 53 hpf with anti-desmin and anti-myosin immunostaining. Boxed areas were enlarged to show double-positive puncta (indicated by carot). White arrows indicate puncta desmin-labeled puncta. G) Quantification of the number of protein aggregates that were immunopositive for both desmin and myosin or H) positive for desmin but not myosin. In box plots, pairs with the same letter indicate a significant differenc

CHAPTER 4: Discussion

Filamin C (FLNC) is muscle-specific gene expressed in cardiomyocytes and skeletal muscle cells (Fujita, Mitsuhashi et al. 2012). Vertebrate Flnc genes contain 49 exons that encode an N-terminal actin-binding domain, 24 immunoglobulin (Ig)-like repeats that form a rod domain, and a C terminal dimerization domain in Ig repeats 24. In the cell, FLNC ensures the stabilization of the actin fiber networks of muscle cells and interacts with several proteins found within the Z-disk (van der Flier and Sonnenberg 2001). To date, different types of mutations within the FLNC gene have been shown to cause progressive myofibrillar myopathies (MFM) or several types of cardiomyopathy (Begay, Graw et al. 2018, Gemelli, Prada et al. 2019). Human FLNC mutations have been identified in several protein domains (Fürst, Goldfarb et al. 2013). With regard to MFM, human FLNC mutations in the actin-binding domain (ABD) lead to weakness and wasting of distal muscles. Mutations located in the rod domain are responsible for proximal myopathy and with typical myofibrillar features which can also involve cardiac and respiratory muscles (Gemelli, Prada et al. 2019). With regard to cardiomyopathy, mutations do not cluster to any particular region of FLNC, and it has been a mystery why different alleles cause different types of cardiomyopathy. Most recently, a novel FLNC truncating mutation was identified as a premature stop codon within exon 45. This mutation tends to cause significant cardiac arrhythmias (Gemelli, Prada et al. 2019, Mangum and Ferns 2019). Model organisms including mice, medaka, and zebrafish have begun to clarify the mechanisms of FLNC mutation that lead to myopathies. In our lab, we used zebrafish to address the role of FLNC in cardiac development by investigating several genetic lines with mutations that target different locations within the gene. To study the loss-of-function phenotype, we investigated embryos homozygous for nonsense alleles: *flnca* $^{exon1-/-}$ and *flncb* $^{exon1-/-}$, in which the stop codon occurs in the actin

binding domain. To compare phenotypes associated with truncation mutants, we investigated *flncb* $^{exon14-/-}$ and *flncb* $^{exon35-/-}$ embryos, with the stop codon found in the Ig repeat regions (Alnefaie 2019). Homozygous *flnca* $^{exon1-/-}$ or *flncb* $^{exon1-/-}$ embryos did not show overt heart phenotypes at 24, 48, or 72 hpf. In contrast, the *flncb* $^{exon14-/-}$ and *flncb* $^{exon35-/-}$ putative truncation mutants exhibited cardiac phenotypes, although they are relatively mild (Alnefaie 2019).

The first aim of this study to analyze heart function by high-speed imaging and provide a quantitative assessment of *in vivo* heart performance capable of detecting subtle functional differences in forming hearts. We found that the cardiac muscle of *flnca* $^{exon1-/-}$ mutant embryos did not develop differences in stroke volume or cardiac output compared to wildtype (Fig 3.3B, C). The heart rate and reverse flow fraction were more variable and tended to be greater in *flnca* $^{exon1-/-}$ mutant embryos at 53 hpf, but these differences were not statistically significant (Fig 3.3 A, D). We conclude that the normal function of Flncb in these mutants was able to functionally compensate for the loss of Flnca. In support of this idea, our prior qRT-PCR data indicates that *flncb* transcripts are upregulated in *flnca* mutants. In contrast, the cardiac muscle of *flncb* $^{exon14-/-}$ mutant embryos displayed a significant decrease in stroke volume and cardiac output (Fig 3.1B, C). This result indicates that wildtype *flnca* was not able to compensate the loss of *flncb*. This finding might be explained if the levels of *flnca* transcription were inadequate to provide the minimal amount of Flnc required by the heart. Intriguingly, qRT-PCR data showed that *flnca* transcription was *not* upregulated in the absence of Flncb. Moreover, in situ hybridization data strongly suggest that absolute levels of *flncb* transcript are much more abundant than *flnca* in normal hearts, suggesting that Flncb function is predominant. Alternatively, if translated, the

truncated Flncb$^{exon14-/-}$ protein might exert a gain-of-function toxic phenotype (Alnefaie 2019). One way to resolve this question is to analyze *flncb* $^{exon1-/-}$ mutant hearts by high-speed video to determine if they are truly fully functional, compared to *flncb* $^{exon14-/-}$ mutant hearts, which are not.

Functional analysis of double mutant *flnca*$^{exon1-/-}$ *flncb*$^{exon14-/-}$ embryos also demonstrated decreased stroke volume and cardiac output(Alnefaie 2019). These data share some phenotypic aspects with those of dilated cardiomyopathy patients, such as poor systolic function which alters the pattern of blood flow, and low cardiac output (Begay, Tharp et al. 2016).

From morpholino studies we expected to see increased RFF in *flncb* mutants, but this was not the case for *flncb* $^{exon14-/-}$ mutants (by video analysis) or for *flncb* $^{exon1-/-}$ mutants (by *in vivo* observation.) Although *flncb*$^{exon14-/-}$ mutants showed adverse effects upon contractility (SV and CO), these were not severe enough to perturb retrograde flow. Thus, impaired RFF is not the automatic consequence of alternations in contractility. The length of endothelial closure is defined as the extent of contact from opposing tissues in the AVJ cardiac wall during the period of atrial systole (Bulk, Bark Jr et al. 2016). In normal hearts, most reverse flow is blocked by the endothelial closure that is briefly maintained at the AVJ just before the atrium begins to relax. Nevertheless, a few cells do trickle back through this region of endothelial closure, to produce the normal brief reverse flow ordinarily observed. The length of endothelial closure will decrease when the atrium expands and the ventricle further contracts. We speculate that the heart is able to adjust the physical length or duration of endothelial closure as a compensatory measure to restrain RF even when contractions are abnormal. Current experiments by Max Hostettor in the lab will measure the length of endothelial closure to investigate this possible explanation.

Investigation of heart function in *flncb*$^{exon35-/-}$ mutants showed that hearts function properly and no functional differences noticed in this mutant group (Fig 3.2). This result was surprising in since *flncb*$^{exon35-/-}$ mutants do show morphological phenotypes (severe pericardial edema and stretched chambers) (Alnefaie 2019). Several hypotheses may explain this result. First, if *flncb*$^{exon35-/-}$ transcripts are not translated or do not contribute any partial function, the morphological phenotype may reflect a Flnc insufficiency. Wildtype *flnca* would still be produced in these mutants and may be sufficient to restore normal contractile function but not sufficient for perfect morphological development. Second, *flncb*$^{exon35-/-}$ transcripts might be translated and produce a protein with partial function or at least no toxic side effects. Third, the genetic background may be obscuring a subtle result. We have noticed that some heterozygous pairs produce more strongly affected heart phenotypes, although in all cases the homozygous embryos can be identified by their muscle paralysis. To discern among these hypotheses, a Western blot is critical to confirm whether the truncated alleles do encode transcripts that are translated. We have a new Flnc N-terminal antibody and Western blots will be done. In addition, we might examine *flncb*$^{exon35-/-}$ embryos at a later timepoint (e.g., 72 hpf) to determine whether normal function at 53 hpf decays over developmental time. In sum, we conclude that the hypothesis of reduced cardiac efficiency was supported only for *flncb*$^{exon14-/-}$ mutants.

Although *flncb*$^{exon35-/-}$ mutant hearts were functional under ideal conditions, we hypothesized that abnormal phenotypes might appear if embryos were placed in a sensitized condition. Therefore, we stressed embryos by raising the temperature of their media to 38 degrees from 40-53 hpf. Video-based analysis of heart function at 53 hpf indicated that stressed mutant embryos revealed a significantly lower stroke volume and cardiac output compared to non-stressed wildtype controls. However, the meaning of this observation is obscured by the fact that stressed

wildtype embryos showed no statistical differences from stressed *flncb*$^{exon35-/-}$ mutant embryos. This finding suggests that our heat stress procedure was too intense and affected all embryos regardless of Flnc status. To resolve the question of compromised function under non-ideal conditions, an alternative approach for stressing hearts undergoing development should be used, such as exposing hearts to pharmacological agents that increase heart rate, or induce high afterload. In another approach, we could evaluate *flncb*$^{exon35-/-}$ mutant embryos that have been co-injected with *flnca* morpholino or sub-threshold doses of morpholino.

The second aim addresses the hypothesis that Flnc is required for normal valve development and morphology. In zebrafish, valve formation progresses through different steps. The early steps (from 33 – 55 hpf) involve the differentiation and specification of endocardial and myocardial cells in the region of the atrioventricular canal. From 33 – 55 hpf, endocardial cells undergo a transition in cell shape from squamous to cuboidal. Later, endocardial cells will undergo an epithelial-to-mesenchymal transition and form valve leaflets (Beis, Bartman et al. 2005). A prior study by Rasha Alnefaie in our lab showed that embryos homozygous for *flnca*$^{exon1-/-}$ displayed no overt cardiac phenotypes at all. Embryos homozygous for *flncb*$^{exon14-/-}$ showed mild to no morphological defects (e.g., cardiac looping was within normal ranges), but when examined at a cellular level, showed impairment of Z-disc formation in early sarcomerogenesis. Embryos homozygous for the *flncb*$^{exon35-/-}$ mutation exhibited more frequent and more severe overt cardiac phenotypes (edema and visual heart morphology), but have not yet been examined for sarcomerogenesis defects. We hypothesized that a correlation may exist between the strength of the cardiac phenotype and the presence of valve defects(Alnefaie 2019). The immunocytochemistry data presented here indicate that homozygous *flncb*$^{exon14-/-}$ and *flncb*$^{exon35-}$

$^{/-}$ embryos both produced significantly fewer differentiated (ALCAM-positive) AVJ endocardial cells. In addition, *flncb*$^{exon35-/-}$ but not *flncb*$^{exon14-/-}$ showed reduction in the cell area of ALCAM-positive endocardial cells in the inferior and superior cushions. Furthermore, the reduction in endocardial cells that observed in *flncb*$^{exon35-/-}$ was not significantly different from *flncb*$^{exon14-/-}$. Neither genotype exhibited significant differences from wildtype in the circularity of ALCAM-positive endocardial cells. Collectively, these studies confirm the presence of valve defects in *flncb* truncation mutants, and suggest that defects in *flncb*$^{exon35-/-}$ embryos are more severe.

The third aim addresses the hypothesis that disruption of FLNC function leads to alteration of *klf2* expression. How biomechanical factors affect gene expression within the embryonic heart is an area of increasing research interest. Mechanotransduction refers to the means by which cells convert information regarding local physical forces into biological outputs, including genetic, biochemical and electrical responses (Miyasaka, Kida et al. 2011). Studies in many animal systems support an essential function for FLNC as a scaffold that helps anchor the sarcomere to cortical actin to other cytoskeletal proteins, consistent with a role in maintaining cell integrity under conditions of force transmission (contraction). In addition, FLNC connects the sarcomere and cytoskeleton to at least two types of transmembrane receptors, consistent with a role in mechanotransductive signaling. We reasoned that alteration of the costamere structure in FLNC mutants would impact contractility, and secondarily impact blood flow patterns. Since our prior study on fish the doubly injected with *flnca* and *flncb* morpholinos showed a statistically increased reverse flow, we anticipated that RFF would be altered in mutants, and the flow-responsive gene *klf2a*.anticipated might exhibit altered expression. Vermot and colleagues (2009) and others have established that endocardial *klf2a* expression of is dependent on the oscillatory flow in the AVJ, otherwise termed the reverse flow fraction (RFF). Specifically, the

reduction in RFF by half was accompanied by a 5-fold decrease in *klf2a* expression (Vermot, Forouhar et al. 2009). A flow-responsive transcriptional change has not been previously demonstrated for *klf2b*, but based upon our recent finding that *klf2b* is expressed in the heart during the developmental window with RF, we analyzed it here. Rasha Alnefaie in our lab previously determined that *flnca*$^{exon1-/-}$ *; flncb*$^{exon14-/-}$ double mutant embryos showed an apparent increase in the variability (though not magnitude) of reverse flow as well as significant decreases in stroke volume and cardiac output (Alnefaie 2019). In our qPCR study, we found that expression levels of *klf2a* and *klf2b* in *flnca*$^{exon1-/-}$ *; flncb*$^{exon14-/-}$ double mutant hearts were significantly decreased. Since RFF was not altered in the double mutants, this finding strongly suggests that Flnc-depletion generates AV phenotypes and alters *klf2a* expression independently of changes in reverse flow. An alternative intriguing possibility is that Flnc helps transmit the RFF-induced mechanosignal to the nucleus to suppress *klf2a* expression (i.e., that it acts downstream of the mechanosignal but upstream of Klf2a). If this is true, a faulty Flnc may not be able to activate *klf2a* to the wildtype levels, leading to *klf2a* decrease even though mechanosignals are normal. However, this hypothesis is tentative since no prior data link Flnc to *klf* expression. An interesting rescue experiment would be to determine whether re-introduction of functional Flnc in a *flnc* mutant would re-instate the normal *klf2* suppression. A second major outcome from these experiements is to identify *klf2b* as a gene transcriptionally influenced by Flnc integrity, although we do not know whether this influence is indirect.

The last aim is to determine which, if any, of the *flnc* mutants develop protein aggregation. Prior studies have proposed that massive formation of intracellular protein aggregates imposes toxic impacts that contribute to the skeletal muscle degeneration observed in myofibrillar myopathy (Fichna, Maruszak et al. 2018). Truncation mutations in *flnc* have the ability to generate protein

aggregates in skeletal muscle of mice and zebrafish (Dalkilic, Schienda et al. 2006, Ruparelia, Zhao et al. 2012), or in mouse hearts (Dalkilic, Schienda et al. 2006). In addition, some human *flnc* truncation mutations affect cardiac or skeletal muscle only while others affect both skeletal and cardiac function (Valdés-Mas, Gutiérrez-Fernández et al. 2014, Brodehl, Ferrier et al. 2016). Genetic mutation of FLNC interaction sites or dimerization domains can lead to its accumulation along with several other muscle proteins in insoluble cytoplasmic aggregates. Protein aggregation is considered a hallmark of MFM and it has been observed in diseased human heart tissue as well. However, the definitive toxicity or disease causality of aggregates has not been demonstrated (Ruparelia, Zhao et al. 2012, Valdés-Mas, Gutiérrez-Fernández et al. 2014) (Ruparelia, Zhao et al. 2012).

In zebrafish, *flncb*$^{exon35-/-}$ allele encodes a nonsense mutation in the 17th Ig domain. If translated, the truncated protein would lack the more C terminal Ig repeats where many of the Flnc protein interaction sites are found. Moreover, it would lack the dimerization domains found near the C-terminus in Ig repeat 24. In contrast to *flncb*$^{exon14-/-}$ mutant embryos, which rarely produced aggregates and did not differ from the wildtype controls (Fig 3.7C), *flncb*$^{exon35-/-}$ mutant embryos showed high level of protein aggregates containing desmin and myosin (Fig 3.7D). Kley and colleagues (2013) evaluated the composition of FLNC aggregates in skeletal muscle fibers using laser capture microdissection followed by proteomics (Kley, Maerkens et al. 2013). Intriguingly, the 31 most prominent proteins do include desmin but do not include myosin or α-actinin (Kley, Maerkens et al. 2013). Moreover in zebrafish studies, Ruparelia found that *flnca*+*flncb* morpholino double knockdown skeletal muscle, which presumably lacked most or all Flnc protein, produced massive numbers of broken skeletal muscle fibers with patches of concentrated myosin near the myosepta (Ruparelia, Zhao et al. 2012). These were interpreted to

represent protein aggregates. Zebrafish *sot/flncb* truncation mutants formed similar protein aggregates, again near the myosepta, but only in the individual muscle fibers that were dissoluting. Immunohistochemistry indicated that all aggregates included both myosin and desmin, but not α-actinin. Later TEM studies of these aggregates indicated they represent the accumulation of filamentous material at the myosepta (Ruparelia, Zhao et al. 2012).. Granular aggregtes were not observed. The authors concluded that these aggregates differ from the typical FLNC-related MFM aggregates, which are granular. They speculate these aggregates may represent the remnants of distintegrated myofibers. In our survey of protein aggregates in zebrafish Flnc mutant hearts, we observed two populations: Some were positive for desmin and myosin, and others were positive only for desmin. In addition, the size and shape of the protein aggregates observed in these two populations are quite difrerent. The desmin-only protein aggregates are a bright round dot or granule whereas the desmin+myosin positive aggregates are more extended, filamentous puncta. This may lead us to conclude that the two populations represent different types of protein aggregates found in FLNC mutant hearts. At present it is not known whether either of these aggregate types contain truncated Flnc protein or any Flnc at all. Ruparelia and colleagues (2016) evaluated a human FLNC truncation construct, named $FLNC^{W2710X}$-eGFP, in zebrafish. $FLNC^{W2710X}$-eGFP contains a premature stop codon in the dimerization domain, Ig-like domain 24. $FLNC^{W2710X}$ represents one of the most common human *flnc* mutations. When injected into 1-cell embryos, the RNA is translated and the resulting $FLNC^{W2710X}$-eGFP can localize to the Z-disc in 48 hpf skeletal muscle. Injection of *$FLNC^{W2710X}$-eGFP* RNA into *flnc a+b* double morpholino embryos amerliorates the skeletal muscle fiber disintegration phenotype, indicating that this protein has at least partial function even though it cannot dimerize. Protein aggregates did form, which were uniformly positive for both myosin

and desmin. The authors suggest that FLNC^{W2710X} may become increasingly sequestered in aggregates over time, resulting in insufficient FLNC at the Z-disk or other required locations. Thus, the authors favor the hypothesis of Flnc insufficiency, rather than aggregate toxicity, as the cause of the muscle phenotypes (Ruparelia, Oorschot et al. 2016).

In humans, several *flnc* mutations in various locations of the rod domain (the Ig domains) result in protein aggregation in the fourth-to-sixth decade of life. Although heterozygous, these patients experienced a slow progression of weakened skeletal muscle, as well as cardiac and respiratory muscle phenotypes (Vorgerd, van der Ven et al. 2005, Kley, Hellenbroich et al. 2007, Valdés-Mas, Gutiérrez-Fernández et al. 2014). A *flnc* mutation in the actin-binding domain (ABD) was involved in distal myopathy characterized by weakness and wasting of distal muscles in the third decade of life (Duff, Tay et al. 2011). The pathomechansims of these mutations in different regions of the Flnc gene are proposed to fall into three categories (Fürst, Goldfarb et al. 2013). First, mutations that cause expression of misfolded FLNC which accumulates in aggregates that eventually overwhelm the ubiquitin proteasome and autophagy pathways, limiting the ability of these pathways to clear the abnormal proteins (the "aggregate-mediated toxicity" mechanism). Second, mutations that do not impact the properties of protein solubility (i.e., do not form aggregates) but rather produce a toxic gain of function by altering how the truncated protein interacts with its binding partners (the "non-aggregate mediated toxicity" mechanism). Third, mutations that cause a premature stop codon and lead to nonsense-mediated decay, generating a shortage of protein which then causes *flnc* insufficiency (the "insufficiency without overt toxic effects" mechanism). Mutations in this third category do not cause the protein aggregation observed in MFM, but only a loss-of-function phenotype as observed in distal myopathy (Fürst, Goldfarb et al. 2013). Haploinsufficiency has been proposed as the most frequent cause for the

distal myopathy and dilated cardiomyopathy (Guergueltcheva, Peeters et al. 2011) and fits with the observation that most affected humans are heterozygous for a mutant allele. Yet, *flnc* haploinsufficiency does not inevitably lead to disease since in more than 12 documented cases, humans with full or partial deletion of the *flnc* gene were identified as healthy. Some authors propose that lack of expression of mutant protein (e.g., NMD) precludes formation of major protein aggregates (Reinstein, Gutierrez-Fernandez et al. 2016). This is not consistent with the extensive presence of aggregates observed in the zebrafish double morpholino knockdown studies of skeletal muscle (Ruparelia, Zhao et al. 2012), but if those aggregates are of a different type than human MFM aggregates, then the hypothesis may stand.

In future studies, it is critical to determine whether the RNA of our *flncb*$^{exon14-/-}$ and *flncb*$^{exon35-/-}$ mutant alleles is translated or not, which may be accomplished by Western blot. In addition, further work should be done to investigate valve differention events in double *flnca*$^{exon1-/-}$*;flncb*$^{exon14-/-}$ embryos, to understand why *klf* transcription is altered even in the absence of changes in RFF. Ours is the first example of such a case. Another interesting future study would be to see if *flnc* mutant groups show arrhythmia at late stage of development. Finally, to confirm our data, zebrafish Flnca and Flncb-specific antibodies could be used in IHC studies to investigate if any translated protein is present in some or all protein aggregates observed in *flncb*$^{exon35-/-}$ mutant alleles.

CHAPTER 5: MATERIAL AND METHODS

Zebrafish Husbandry

Adult zebrafish and fry were raised at a temperature range of 27-28°C. Brine and flakes were given to adult zebrafish on a daily basis while the babies were given Ziegler's liquid diet. When the baby zebrafish were about five days post fertilization, they were introduced to our recirculating water system. At first, the babies zebrafish were put into no-flow water and then shifted to slow flow water at 14 days. At three months, they were moved to regular flowing water. They were given liquid diet up to the age of 3 months. However, flakes were added into the baby zebrafish diet when they were two weeks old. Breeding started at three months of post fertilization. At the age of two years or after the fish were replenished due to reduced fertility. The old fish were humanely euthanized based on the ACUC (Animal Care and Use Committee) approved guidelines. WIK wild type lines were used. Developmental staging was performed according to Kimmel and colleagues (Kimmel, Ballard et al. 1995).

RNA Extraction

53 hpf embryo hearts were dissected by through pipetting (7 to 8 times with 2 mL pipette). Hearts were transferred to 1.5 ml Eppendorf tubes. These tubes contained LB15 medium in 10 percent FBS (fetal bovine serum). 250 µl TRIzol reagent was used to dissect and homogenize about 10-15 hearts from each genotype (CA, Invitrogen, USA and Carlsbad). Isolation of the total RNA followed the protocol provided by the manufacturer. In brief, extraction of total RNA was performed through the addition of phenol: chloroform, after which the RNA was precipitated with about one volume of isopropanol in order to eliminate salts. A washing step followed, in which 75 percent ETOH was applied. RNA pellets were resuspended in 13 µl of nuclease-free water. Finally, 1 µl Invitrogen DNase l was added to eliminate genomic DNA.

cDNA Synthesis

For the determination of RNA concentration and quality, an aliquot of each extract was used for spectrophotometry. In this research, samples of RNA with a 260:280 ratio within a range of 1.8-2.0 and a 260:230 ratio between 1 and 3 were used. Subsequently, cDNA synthesis reactions were performed using Oligo(dT)12-18 primer (Invitrogen) together with about 1-2 µg RNA (in a final reaction volume of 20 µl). Reactions contained 1µl AMV reverse transcriptase based on the manufacturer's instructions.

PCR and Gel Electrophoresis:

GoTaq® (Promega) was used to carry out PCR. Agarose gel electrophoresis was done according to standard protocols. A 0.8 percent Gene Pure LE agarose gel was used for most of the tests that were conducted. TAE buffer was used as a gel buffer and running buffer. GeneRuler 1kb DNA Ladder Plus was used (Fermentas SM1331). Ethidium bromide was added to gels when cast. In addition, ethidium bromide was added into the running buffer prior to the start of the gel. Image Lab software and a GelDoc (Bio-Rad) imager were used to record the gels. A light box and razor blade were used to extract bands where necessary. DNA extraction from gel bands was achieved through the use of the Qiagen (QIAEX®ll Gel Extraction Kit).

Oligonucleotides

Synthesis of all oligonucleotide primers was done by IDTA.

Standard RT-PCR templates were used to verify specificity of primer sets using wildtype cardiac cDNA as the template. cDNA from embryonic zebrafish was used to verify that only a single band of the anticipated size was produced. The primers were used in all reactions at a dilution ratio of 1:5 from 100 Mm stock as indicated in Table 5.1.

.

Table 5.1: Primers for Quantitative PCR and PCRs

Primer name	Number in primer file	Primer sequence
Elongation factor 1-alpha (*efa1*)	546 Fwd	5'-CGGTGACAACATGCTGGAGG-'3
efa1	547 Rev	3'-ACC AGT CTCCACACGACCCA-'5
klf2a	244 Fwd	5'-GCCAGAGCTATCAAGGCAAC-'3
klf2a	245 Rev	3'-TGCCACATCCAGAAAAAGTG-'5
klf2b	245 Fwd	5'-GCCATGTATGAGGAGGCAAT-'3
klf2b	246 Rev	3'-CCTCCCAGTTGCAGTGGTAT-'5
Flnca	525 Fwd	5'-AGTTTCTGGACAGGGAGAGA-'3
Flnca	526 Rev.	3'-CCCAGAATCAGCTTCAGGTT-'5
Flncb	533 Fwd	5'-ACGATGAAGACGCCAGAAAG-'3
Flncb	534 Rev.	5'-CAGTCCCTGTGGAAGTTGTT-'3

qPCR

A Light Cycler 480 thermal cycler and Light Cycler Fast Start DNA Master Plus SYBR Green I reaction mix were used to carry out qRT-PCR (quantitative reverse transcription polymerase chain reaction). Each 10 µl reaction contained: 5 µl 2× SYBR green master mixture, 1 µl of RT reaction, 2 µl of every reverse and forward primers (each at a concentration of 5 µM). The samples were run in triplicate in 384-well plates that were optically clear. The parameters of polymerase chain reaction cycling were comprised of an initial denaturation at a temperature of 95°C for 5 minutes; 45 denaturation cycles at a temperature of 95°C for 20 sec; annealing at a temperature of 55°C for 20 sec, and finally extension at a temperature of 72°C for 15 sec. After each run, the melting temperature of PCR products was analyzed. Compilation of the real-time PCR generated data was done and amplification efficiency (E) of the PCR reaction was calculated for every pair of primers.

Following the method of Muller et al. (2002), a linear regression analysis based on a dilution series was used to determine the E=10(-1/slope) value(Muller, Janovjak et al. 2002). We stipulated that every acceptable amplification must have a polymerase chain reaction efficiency value of 1.90-2.2. Tang et al. (2007) argue that every primer pair's efficiency (E) should be used in conjunction with the cycle threshold values in order to determine the value of relative gene expression for every transcript, as described in the following equation:

$$RQ = \frac{(E_{target})^{\Delta Ct\,(target)}}{(E_{reference})^{\Delta Ct\,(reference)}}$$

The number of cycles that are necessary for fluorescence to cross over a certain detection threshold level is called the cycle threshold or Ct value. It is related to the number of templates that exist in the reaction, as noted by Walker (2002). The significant differences in expression of *klf2a* and *klf2b* between double *flnca*$^{exon1-/-}$, *flncb*$^{exon14-/-}$ or wild type heart samples were determined using the Student's t-test.

Functional analysis of zebrafish heart by high-speed videos

Live wildtype,*flnca*$^{exon1-/-}$, ,*flncb*$^{exon14-/-}$,*flncb*$^{exo35-/-}$ or stressed *flncb*$^{exo35-/-}$ zebrafish embryos were positioned in 1.5 percent of low melting agarose gel with the ventral side facing upwards.

Imaging: A high speed camera (Photron,FASTCAM SA3) was used to record videos. The camera (Photron,FASTCAM SA3) was mounted onto a stereomicroscope containing the SZX-AL20X lens attachment. Recordings were captured at 2500 fps (frames per second) under a bright field lighting that had a 1,310 pixels/mm resolution (videos were about 3 sec long, enough to capture ~3-4 heartbeats). The camera was controlled using Photron FASTCAM Viewer software that also was used to save image files.

Image Processing: In-house MATLAB interface was used to carry out data analysis and image processing. Brennan Johnson's methods were used to process the images as described (Johnson 2014).

Image Analysis: First, raw images were registered to remove artifacts produced by shaking during image acquisition. Image sequences were normalized to account for light intensity in different frames, and presented as a spatiotemporal plot (ST). The analysis of image sequences for heart rate, diameter, and velocity followed. These data were used to calculate all subseqeunt data. Stroke volume (SV) represents the net blood volume that is pumped to the rest of the body in every cardiac cycle. It is calculated through the integration of the flow rate curve across the whole cardiac cycle. To obtain the cardiac output, stroke volume is multiplied by heart rate. The total blood moving in reverse path in the AVC in a single cardiac cycle is called the reverse or retrograde flow fraction (RF). Here, RF is calculated as the ratio of reverse-moving blood volume divided by forward-moving blood volume per heartbeat. Statistical comparisons used Tukey and ANOVA tests with version 12.0 of SigmaPlot software. $P < 0.05$ was considered to be significant.

Immunocytochemistry (ICC)

Hearts were dissected as above. Heart samples were then placed on slides coated with polylysine. An ImmEdge pen was used to encircle the samples so as to form a well that could retain a small amount of fluid. Samples were then placed into a humidified chamber. To each well, we added 20 µl of LB15 media (GE Healthcare SH30525.02) in 10 percent FBS (fetal bovine serum). Each heart was fixed with 4 percent PFA for a period of 40 minutes at room temperature. PBST (phosphate buffered saline with 2% Triton) was then used to rinse the hearts. Hearts were washed 3 times for 5 minutes, then blocked in 10 percent of sheep serum for an hour in PBST at

room temperature. Heart samples were then incubated with primary antibody, then washed and re-incubated by secondary antibody. Primary antibodies included anti-Alcam (zn8; DSHB) at a 1:10 dilution , anti-desmin (Novusbio SI18-00) at a 1:80 dilution and anti-myosin (F59; DSHB) at a 1:10 dilution in 10 percent of sheep serum/PBST. Primary antibodies were applied for an hour at room temperature in the humidified chamber. Hearts were washed 3 times using PBST for 5 minutes. Then, secondary antibodies included: Alexa Fluor 546 goat anti-rabbit (Invitrogen 584959) at a 1:500 dilution, Alexa Fluor 546 goat anti-mouse at a 1: 200 dilution, and Zenon Alex flour 488 anti-mouse antibody (Invitrogen 1985263) at a dilution of 1:200. Secondary antibodies were applied for an hour followed by washing step (PBST 3 times for 5 minutes). Finally, to each well we added 10 µl of 70 percent glycerol to assist in mounting the heart upon a cover slip. A laser scanning confocal microscope (Zeiss LSM 800) was used to image the heart samples. The microscope resides in the A/Z building room W5.

Establishment of mutant crosses

The transgenic line *Tg(fli1:eGFP)]* that expresses GFP in endothelial and endocardial cells, created by Yang and Xu (2012), was crossed with *flncb*$^{exon14+/-}$ adults or *flncb*$^{exon\ 35+/-}$ adults to obtain heterozygous with *flncb*$^{exon14+/-}$ offspring or *flncb*$^{exon\ 35+/-}$ offspring which express *fli1:eGFP*. When *flncb*$^{exon14-/-}$ fish were adults, it was crossed with adult homozygous mutant *flncb*$^{exon14-/-}$ fish in order to obtain homozygous mutant *flncb*$^{exon14-/-}$;*Tg(fli1:eGFP)* to be expermentily analysed. Whereas *flncb*$^{exon35-/-}$dose not survive to adulthood so we crossed two *flncb*$^{exon35-/+}$;*Tg(fli1:eGFP*) and select the embryos that showed the heart phenotype and express *fli1:eGFP*. to be experimentally analyzed.

Zebrafish heart structure analysis

Area, cell number and circularity:

The labelling of cell membranes was achieved by immunocytochemistry using anti-Alcam antibody. This procedure was used to measure the superior and inferior cell area of mutant heart and wildtype samples at 53 hpf. Image J software was used to calculate the cross-sectional area of the cell. The area of five cells was averaged and counted as a single sample. One-way ANOVA was used to analyze the variations among groups. This was followed by Tukey tests that were conducted using version 12.0 of SigmaPlot software. $P < 0.05$ was considered to be significant.

Genotyping filamin C various alleles mutant zebrafish that express fli1:eGFP:

Adult fish that aged 2-4 months were fin clipped and their genomic DNA extracted by the method of Meeker et al. (2007), Genotyping was then carried out by PCR. Table 5.2 shows the list of the primer sequences used for each allele. The PCR products were separated on a 0.8 percent agarose gel. Bands were cut out and DNA recovered using the QIAquick Gel Extraction Kit Cat (Qiagen 28706) . Purified DNA samples were submitted to Quintarabio for sequencing. See also https://www.qiuntarabio.com/servive/dna sequencing.

.

Table 5.2: Genotyping mutant line PCR primer sequences

Primer name	Number in primer file	Primer sequence
flnca sa24724 Fwd	484 Fwd	5'-GGCACAGACCTTGGAGAAGA-'3
flnca sa24724 Rev	485 Rev	5'-CCCTGTCCAGAAACTCCAGC-'3
flncb sa15601 Fwd	482 Fwd	5'-AAAGGGGGCACGAAAACATC-'3
flncb sa15601 Rev	483 Rev	5'-AAACCAGTTTGATGTGTTCCCT-'3
flncb sa11171 Fwd	470 Fwd	5'-GTGGAGCTGGAAGAGGACAG'-3
flncb sa11171 Rev	471 Rev	5-TTGATGGGCTTGATGGGTAT-3
flncb sa20217 Fwd	548 Fwd	5'-CTCCCAGGTGGTCTGTCATT-'3
flncb sa20217 Rev	549 Rev	5'-TTGCCCTCTCTTGTTCATCC-'3

REFERENCES

Ackermann, G. E. and B. H. Paw (2003). "Zebrafish: a genetic model for vertebrate organogenesis and human disorders." Front Biosci **8**(1): d1227-1253.

Ader, F., et al. "FLNC pathogenic variants in patients with cardiomyopathies: Prevalence and genotype-phenotype correlations." Clinical Genetics.

Aguzzi, A. and T. O'Connor (2010). "Protein aggregation diseases: pathogenicity and therapeutic perspectives." Nature reviews Drug discovery **9**(3): 237.

Aikawa, E., et al. (2006). "Human semilunar cardiac valve remodeling by activated cells from fetus to adult: implications for postnatal adaptation, pathology, and tissue engineering." Circulation **113**(10): 1344-1352.

Alnefaie, R. M. (2019). "Characterization of zebrafish models of filamin C related cardiomyopathy."

Andrés-Delgado, L. and N. Mercader (2016). "Interplay between cardiac function and heart development." Biochimica et Biophysica Acta (BBA)-Molecular Cell Research **1863**(7): 1707-1716.

Asnani, A. and R. T. Peterson (2014). "The zebrafish as a tool to identify novel therapies for human cardiovascular disease." Disease Models & Mechanisms **7**(7): 763.

Atherton, P., et al. (2016). "Mechanosensitive components of integrin adhesions: Role of vinculin." Experimental cell research **343**(1): 21-27.

Baker, K., et al. (1997). "Defective “pacemaker” current (Ih) in a zebrafish mutant with a slow heart rate." Proceedings of the National Academy of Sciences **94**(9): 4554-4559.

Bakkers, J. (2011). "Zebrafish as a model to study cardiac development and human cardiac disease." Cardiovascular research **91**(2): 279-288.

Banjo, T., et al. (2013). "Haemodynamically dependent valvulogenesis of zebrafish heart is mediated by flow-dependent expression of miR-21." Nature communications **4**: 1978.

Begay, R. L., et al. (2018). "Filamin C truncation mutations are associated with arrhythmogenic dilated cardiomyopathy and changes in the cell–cell adhesion structures." JACC: Clinical Electrophysiology **4**(4): 504-514.

Begay, R. L., et al. (2016). "FLNC Gene Splice Mutations Cause DilatedáCardiomyopathy." JACC: Basic to Translational Science **1**(5): 344-359.

Beis, D., et al. (2005). "Genetic and cellular analyses of zebrafish atrioventricular cushion and valve development." Development **132**(18): 4193-4204.

Bialkowska, A. B., et al. (2017). "Krüppel-like factors in mammalian stem cells and development." Development **144**(5): 737-754.

Boselli, F., et al. (2015). "Blood flow mechanics in cardiovascular development." Cellular and molecular life sciences **72**(13): 2545-2559.

Bournele, D. and D. Beis (2016). "Zebrafish models of cardiovascular disease." Heart failure reviews **21**(6): 803-813.

Brodehl, A., et al. (2016). "Mutations in FLNC are associated with familial restrictive cardiomyopathy." Human mutation **37**(3): 269-279.

Bulk, A., et al. (2016). "Mechanisms influencing retrograde flow in the atrioventricular canal during early embryonic cardiogenesis." Journal of biomechanics **49**(14): 3162-3167.

Carpio, Y. and M. P. Estrada (2006). "Zebrafish as a Genetic Model organism." Biotecnología Aplicada **23**(4): 265-270.

Chakarova, C., et al. (2000). "Genomic structure and fine mapping of the two human filamin gene paralogues FLNB and FLNC and comparative analysis of the filamin gene family." Human genetics **107**(6): 597.

Chi, N. C., et al. (2008). "Genetic and physiologic dissection of the vertebrate cardiac conduction system." PLoS biology **6**(5): e109.

Chien, S. (2007). "Mechanotransduction and endothelial cell homeostasis: the wisdom of the cell." American Journal of Physiology-Heart and Circulatory Physiology **292**(3): H1209-H1224.

Cotelli, F., et al. (1988). "Structure and composition of the fish egg chorion (Carassius auratus)." Journal of ultrastructure and molecular structure research **99**(1): 70-78.

Dahme, T., et al. (2009). "Fishing for the genetic basis of cardiovascular disease." Disease models & mechanisms **2**(1-2): 18-22.

Dalkilic, I., et al. (2006). "Loss of FilaminC (FLNc) results in severe defects in myogenesis and myotube structure." Molecular and cellular biology **26**(17): 6522-6534.

Dekker, R. J., et al. (2006). "KLF2 provokes a gene expression pattern that establishes functional quiescent differentiation of the endothelium." Blood **107**(11): 4354-4363.

Dekker, R. J., et al. (2005). "Endothelial KLF2 links local arterial shear stress levels to the expression of vascular tone-regulating genes." The American journal of pathology **167**(2): 609-618.

Dietrich, A.-C., et al. (2014). "Blood flow and Bmp signaling control endocardial chamber morphogenesis." Developmental cell **30**(4): 367-377.

Dooley, K. and L. I. Zon (2000). "Zebrafish: a model system for the study of human disease." Curr Opin Genet Dev **10**(3): 252-256.

Duff, R. M., et al. (2011). "Mutations in the N-terminal actin-binding domain of filamin C cause a distal myopathy." The American Journal of Human Genetics **88**(6): 729-740.

Fan, Y., et al. (2017). "Krüppel-like factors and vascular wall homeostasis." Journal of molecular cell biology **9**(5): 352-363.

Fichna, J. P., et al. (2018). "Myofibrillar myopathy in the genomic context." Journal of applied genetics **59**(4): 431-439.

Fujita, M., et al. (2012). "Filamin C plays an essential role in the maintenance of the structural integrity of cardiac and skeletal muscles, revealed by the medaka mutant zacro." Developmental biology **361**(1): 79-89.

Fukuda, R., et al. (2019). "Mechanical Forces Regulate Cardiomyocyte Myofilament Maturation via the VCL-SSH1-CFL Axis." Developmental cell.

Fürst, D. O., et al. (2013). "Filamin C-related myopathies: pathology and mechanisms." Acta neuropathologica **125**(1): 33-46.

Gardiner, M. R., et al. (2007). "A global role for zebrafish klf4 in embryonic erythropoiesis." Mechanisms of development **124**(9-10): 762-774.

Garrity, D. M., et al. (2002). "The heartstrings mutation in zebrafish causes heart/fin Tbx5 deficiency syndrome." Development **129**(19): 4635-4645.

Gemelli, C., et al. (2019). "A novel mutation in the N-terminal acting-binding domain of Filamin C protein causing a distal myofibrillar myopathy." Journal of the neurological sciences **398**: 75-78.

Gijsen, F., et al. (2013). "Shear stress and advanced atherosclerosis in human coronary arteries." Journal of biomechanics **46**(2): 240-247.

Go, A. S., et al. (2013). "Executive summary: heart disease and stroke statistics—2013 update: a report from the American Heart Association." Circulation **127**(1): 143-152.

Gomer, R. H. and E. Lazarides (1981). "The synthesis and deployment of filamin in chicken skeletal muscle." Cell **23**(2): 524-532.

Grimes, A. C., et al. (2006). "Solving an enigma: arterial pole development in the zebrafish heart." Developmental biology **290**(2): 265-276.

Groenendijk, B. C. W., et al. (2005). "Changes in shear stress–related gene expression after experimentally altered venous return in the chicken embryo." Circulation research **96**(12): 1291-1298.

Guergueltcheva, V., et al. (2011). "Distal myopathy with upper limb predominance caused by filamin C haploinsufficiency." Neurology **77**(24): 2105-2114.

Gunawan, F., et al. (2019). "Focal adhesions are essential to drive zebrafish heart valve morphogenesis." J Cell Biol **218**(3): 1039-1054.

Haack, T. and S. Abdelilah-Seyfried (2016). "The force within: endocardial development, mechanotransduction and signalling during cardiac morphogenesis." Development **143**(3): 373-386.

Hami, D., et al. (2011). "Zebrafish cardiac development requires a conserved secondary heart field." Development **138**(11): 2389-2398.

Hogers, B., et al. (1999). "Extraembryonic venous obstructions lead to cardiovascular malformations and can be embryolethal." Cardiovascular research **41**(1): 87-99.

Hove, J. R., et al. (2003). "Intracardiac fluid forces are an essential epigenetic factor for embryonic cardiogenesis." Nature **421**(6919): 172.

Howe, K., et al. (2013). "The zebrafish reference genome sequence and its relationship to the human genome." Nature **496**(7446): 498.

Huang, C. J., et al. (2003). "Germ-line transmission of a myocardium-specific GFP transgene reveals critical regulatory elements in the cardiac myosin light chain 2 promoter of zebrafish." Developmental dynamics: an official publication of the American Association of Anatomists **228**(1): 30-40.

Hurlstone, A. F. L., et al. (2003). "The Wnt/β-catenin pathway regulates cardiac valve formation." Nature **425**(6958): 633.

Johnson, B. M. (2014). "Quantifying function in the zebrafish embryonic heart: a study on the role of timed mechanical cues."

Keßler, M., et al. (2012). "Ion flux dependent and independent functions of ion channels in the vertebrate heart: lessons learned from zebrafish." Stem cells international **2012**.

Kimmel, C. B., et al. (1995). "Stages of embryonic development of the zebrafish." Developmental Dynamics **203**(3): 253-310.

Kley, R. A., et al. (2007). "Clinical and morphological phenotype of the filamin myopathy: a study of 31 German patients." Brain **130**(12): 3250-3264.

Kley, R. A., et al. (2013). "A combined laser microdissection and mass spectrometry approach reveals new disease relevant proteins accumulating in aggregates of filaminopathy patients." Molecular & cellular proteomics **12**(1): 215-227.

Knight, H. G. and D. Yelon (2016). Utilizing zebrafish to understand second heart field development. Etiology and Morphogenesis of Congenital Heart Disease, Springer, Tokyo**:** 193-199.

Lee, J. S., et al. (2006). "Klf2 is an essential regulator of vascular hemodynamic forces in vivo." Developmental cell **11**(6): 845-857.

Lin, S., et al. (2013). "Zebrafish: An In Vivo Model for Nano EHS Studies." Small **9**(9-10): 1608-1618.

Lindsey, S. E., et al. (2014). "Mechanical regulation of cardiac development." Frontiers in physiology **5**: 318.

Linnemann, A., et al. (2010). "The sarcomeric Z-disc component myopodin is a multiadapter protein that interacts with filamin and α-actinin." European journal of cell biology **89**(9): 681-692.

Liu, J. and D. Y. R. Stainier (2012). "Zebrafish in the study of early cardiac development." Circulation research **110**(6): 870-874.

Liu, K., et al. (2019). "Expanding the CRISPR Toolbox in Zebrafish for Studying Development and Disease." Frontiers in cell and developmental biology **7**.

Lu, F., et al. (2016). "Transcriptional regulation of heart development in zebrafish." Journal of cardiovascular development and disease **3**(2): 14.

Luan, X., et al. (2010). "A novel heterozygous deletion–insertion mutation (2695–2712 del/GTTTGT ins) in exon 18 of the filamin C gene causes filaminopathy in a large Chinese family." Neuromuscular Disorders **20**(6): 390-396.

Mangum, K. D. and S. J. Ferns (2019). "A novel familial truncating mutation in the filamin C gene associated with cardiac arrhythmias." European journal of medical genetics **62**(4): 282-285.

Matsui, T., et al. (2007). "miles-apart-Mediated regulation of cell–fibronectin interaction and myocardial migration in zebrafish." Nature Reviews Cardiology **4**(S1): S77.

McConnell, B. B. and V. W. Yang (2010). "Mammalian Krüppel-like factors in health and diseases." Physiological reviews **90**(4): 1337-1381.

Merlo, M., et al. (2018). "Evolving concepts in dilated cardiomyopathy." European journal of heart failure **20**(2): 228-239.

Meyer, A. and M. Schartl (1999). "Gene and genome duplications in vertebrates: the one-to-four (-to-eight in fish) rule and the evolution of novel gene functions." Current opinion in cell biology **11**(6): 699-704.

Meyers, J. R. (2018). "Zebrafish: Development of a Vertebrate Model Organism." Current Protocols Essential Laboratory Techniques **16**(1): e19.

Midgett, M. and S. Rugonyi (2014). "Congenital heart malformations induced by hemodynamic altering surgical interventions." Frontiers in physiology **5**: 287.

Miller, I. J. and J. J. Bieker (1993). "A novel, erythroid cell-specific murine transcription factor that binds to the CACCC element and is related to the Krüppel family of nuclear proteins." Molecular and cellular biology **13**(5): 2776-2786.

Miyasaka, K. Y., et al. (2011). "Heartbeat regulates cardiogenesis by suppressing retinoic acid signaling via expression of miR-143." Mechanisms of development **128**(1-2): 18-28.

Muller, P. Y., et al. (2002). "Processing of gene expression data generated by quantitative real-time RT PCR (vol 32, pg 1378, 2002)." Biotechniques **33**(3): 514-514.

Nagai, R., et al. (2009). The biology of Krüppel-like factors, Springer.

Nemtsas, P., et al. (2010). "Adult zebrafish heart as a model for human heart? An electrophysiological study." Journal of molecular and cellular cardiology **48**(1): 161-171.

Nguyen, C. T., et al. (2008). "Zebrafish as a model for cardiovascular development and disease." Drug Discovery Today: Disease Models **5**(3): 135-140.

Oates, A. C., et al. (2001). "The zebrafish klf gene family." Blood **98**(6): 1792-1801.

Oishi, Y. and I. Manabe (2018). "Krüppel-like factors in metabolic homeostasis and cardiometabolic disease." Frontiers in cardiovascular medicine **5**.

Ortiz-Genga, M. F., et al. (2016). "Truncating FLNC mutations are associated with high-risk dilated and arrhythmogenic cardiomyopathies." Journal of the American College of Cardiology **68**(22): 2440-2451.

Parmar, K. M., et al. (2006). "Integration of flow-dependent endothelial phenotypes by Kruppel-like factor 2." The Journal of clinical investigation **116**(1): 49-58.

Pelster, B. and W. W. Burggren (1996). "Disruption of hemoglobin oxygen transport does not impact oxygen-dependent physiological processes in developing embryos of zebra fish (Danio rerio)." Circulation research **79**(2): 358-362.

Petridou, N. I., et al. (2017). "Multiscale force sensing in development." Nature cell biology **19**(6): 581.

Poon, K.-L., et al. (2016). "Development of the cardiac conduction system in zebrafish." Gene Expression Patterns **21**(2): 89-96.

Poon, K. L. and T. Brand (2013). "The zebrafish model system in cardiovascular research: A tiny fish with mighty prospects." Glob Cardiol Sci Pract **2013**(1): 9-28.

Poon, K. L., et al. (2010). "Zebrafish cardiac enhancer trap lines: new tools for in vivo studies of cardiovascular development and disease." Developmental dynamics: an official publication of the American Association of Anatomists **239**(3): 914-926.

Reinstein, E., et al. (2016). "Congenital dilated cardiomyopathy caused by biallelic mutations in Filamin C." European Journal of Human Genetics **24**(12): 1792.

Reischauer, S., et al. (2014). "Actin binding GFP allows 4D in vivo imaging of myofilament dynamics in the zebrafish heart and the identification of Erbb2 signaling as a remodeling factor of myofibril architecture." Circulation research **115**(10): 845-856.

Rocke, J., et al. (2009). "The zebrafish as a novel tool for cardiovascular drug discovery." Recent patents on cardiovascular drug discovery **4**(1): 1-5.

Ruparelia, A. A., et al. (2016). "FLNC myofibrillar myopathy results from impaired autophagy and protein insufficiency." Human molecular genetics **25**(11): 2131-2142.

Ruparelia, A. A., et al. (2012). "Characterization and investigation of zebrafish models of filamin-related myofibrillar myopathy." Human molecular genetics **21**(18): 4073-4083.

Sanoja, A. J., et al. (2018). "Exome sequencing identifies FLNC and ADD3 variants in a family with cardiomyopathy."

Santhanakrishnan, A. and L. A. Miller (2011). "Fluid dynamics of heart development." Cell biochemistry and biophysics **61**(1): 1-22.

Scherz, P. J., et al. (2008). "High-speed imaging of developing heart valves reveals interplay of morphogenesis and function." Development **135**(6): 1179-1187.

Schiffhauer, E. S. and D. N. Robinson (2017). "Mechanochemical signaling directs cell-shape change." Biophysical journal **112**(2): 207-214.

Schröder, R. and B. Schoser (2009). "Myofibrillar myopathies: a clinical and myopathological guide." Brain pathology **19**(3): 483-492.

Sehnert, A. J., et al. (2002). "Cardiac troponin T is essential in sarcomere assembly and cardiac contractility." Nature genetics **31**(1): 106.

Seto, S.-W., et al. (2015). "Zebrafish models of cardiovascular diseases and their applications in herbal medicine research." European journal of pharmacology **768**: 77-86.

Sidhwani, P. and D. Yelon (2019). "Fluid forces shape the embryonic heart: Insights from zebrafish." Current topics in developmental biology **132**: 395-416.

Spence, R., et al. (2008). "The behaviour and ecology of the zebrafish, Danio rerio." Biological Reviews **83**(1): 13-34.

Stainier, D. Y. R. (2001). "Zebrafish genetics and vertebrate heart formation." Nature Reviews Genetics **2**(1): 39.

Stainier, D. Y. R. and M. C. Fishman (1994). "The zebrafish as a model system to study cardiovascular development." Trends in cardiovascular medicine **4**(5): 207-212.

Staudt, D. and D. Stainier (2012). "Uncovering the molecular and cellular mechanisms of heart development using the zebrafish." Annual review of genetics **46**: 397-418.

Steed, E., et al. (2016). "Hemodynamics driven cardiac valve morphogenesis." Biochimica et Biophysica Acta (BBA)-Molecular Cell Research **1863**(7): 1760-1766.

Stossel, T. P., et al. (2001). "Filamins as integrators of cell mechanics and signalling." Nature reviews Molecular cell biology **2**(2): 138.

Tasca, G., et al. (2012). "Novel FLNC mutation in a patient with myofibrillar myopathy in combination with late-onset cerebellar ataxia." Muscle & nerve **46**(2): 275-282.

Thisse, B., et al. (2001). "Expression of the zebrafish genome during embryogenesis." ZFIN direct data submission.

Thisse, B. and C. Thisse (2004). "Fast release clones: a high throughput expression analysis." ZFIN direct data submission **2004**.

Thompson, T. G., et al. (2000). "Filamin 2 (FLN2): a muscle-specific sarcoglycan interacting protein." J Cell Biol **148**(1): 115-126.

Tu, S. and N. C. Chi (2012). "Zebrafish models in cardiac development and congenital heart birth defects." Differentiation **84**(1): 4-16.

Valdés-Mas, R., et al. (2014). "Mutations in filamin C cause a new form of familial hypertrophic cardiomyopathy." Nature communications **5**: 5326.

van der Flier, A. and A. Sonnenberg (2001). "Structural and functional aspects of filamins." Biochimica et Biophysica Acta (BBA)-Molecular Cell Research **1538**(2-3): 99-117.

van der Ven, P. F. M., et al. (2000). "Characterization of muscle filamin isoforms suggests a possible role of γ-filamin/ABP-L in sarcomeric Z-disc formation." Cell motility and the cytoskeleton **45**(2): 149-162.

van der Ven, P. F. M., et al. (2000). "Indications for a novel muscular dystrophy pathway: γ-filamin, the muscle-specific filamin isoform, interacts with myotilin." The Journal of cell biology **151**(2): 235-248.

Vermot, J., et al. (2009). "Reversing blood flows act through klf2a to ensure normal valvulogenesis in the developing heart." PLoS biology **7**(11): e1000246.

Vorgerd, M., et al. (2005). "L? we T, Kley RA, Schr? der R, Lochm? ller H, Himmel M, Koehler K, FUrst DO, Huebner A: A mutation in the dimerization domain of filamin c causes a novel type of autosomal dominant myofibrillar myopathy." Am J Hum Genet **77**: 297-304.

Walsh, E. C. and D. Y. R. Stainier (2001). "UDP-glucose dehydrogenase required for cardiac valve formation in zebrafish." Science **293**(5535): 1670-1673.

Watkins, H., et al. (2011). "Inherited cardiomyopathies." New England Journal of Medicine **364**(17): 1643-1656.

Yalcin, H. C., et al. (2017). "Heart function and hemodynamic analysis for zebrafish embryos." Developmental Dynamics **246**(11): 868-880.

Yang, H., et al. (2016). "Dynamic myofibrillar remodeling in live cardiomyocytes under static stretch." Scientific reports **6**: 20674.

Yang, J. and X. Xu (2012). "α-Actinin2 is required for the lateral alignment of Z discs and ventricular chamber enlargement during zebrafish cardiogenesis." The FASEB Journal **26**(10): 4230-4242.

Yelon, D. (2001). "Cardiac patterning and morphogenesis in zebrafish." Developmental Dynamics **222**(4): 552-563.

Yokoi, H., et al. (2009). "Expression profiling of zebrafish sox9 mutants reveals that Sox9 is required for retinal differentiation." Developmental biology **329**(1): 1-15.

Zeller, M. J. (2015). "The impact of shear rate and reverse flow on cardiac morphogenesis and gene expression in the embryonic zebrafish heart."

Zhang, P., et al. (2005). "A functional screen for Krüppel-like factors that regulate the human γ-globin gene through the CACCC promoter element." Blood Cells, Molecules, and Diseases **35**(2): 227-235.